Supplementary material
Enhancing the electronic and photocatalytic properties of $(SnO_2)_n/(TiO_2)_m$ oxide superlattices for efficient hydrogen production : a first-principles study.

Najwa Harrati*[a], Bastien Casier[a], and Adlane Sayede†[a]

[1]Univ. Artois, UMR 8181, Unité de Catalyse et de Chimie du Solide (UCCS), F-62300 Lens, France

Supplementary Equations

HSE06 functional

The hybrid Heyd-Scuseria-Ernzerhof (HSE06) functional describes the electron-electron interaction in terms of long-range (LR) and short-range (SR) parts. It combines the exact Hartree-Fock exchange $\alpha E_x^{\mathrm{HF,\ SR}}(\omega)$ with the PBE short-range exchange $E_x^{\mathrm{PBE,\ SR}}$, including the full PBE correlation E_c^{PBE}. The expression for E_{xc}^{HSE} is :

$$E_{xc}^{\mathrm{HSE}} = \alpha E_x^{\mathrm{HF,\ SR}}(\omega) + (1-\alpha)E_x^{\mathrm{PBE,\ SR}}(\omega) + (1-\alpha)E_x^{\mathrm{PBE,\ LR}}(\omega) + \alpha E_c^{\mathrm{PBE}}(\omega) \quad (1)$$

where α and ω are the mixing and screening coefficients, respectively. we set these coefficients to $\alpha = 0.25$ and $\omega = 0.2\ \mathring{A}^{-1}$ to obtain the bandgaps for SnO_2 and TiO_2 systems close to the experimental values.

Photocatalytic properties

For superlattices, such equations need to be rescaled according to their stoichiometry.

For the $(SnO_2)_{(2)}/(TiO_2)_{(2)}$ superlattice :

$$E_{\mathrm{VBM}}^{(SnO_2)_{(2)}/(TiO_2)_{(2)}} = \left((\chi_{\mathrm{Sn}}^2\chi_{\mathrm{Ti}}^2\chi_{\mathrm{O}}^8)^{\frac{1}{12}}\right) - E_0 + \frac{1}{2}E_g \quad (2)$$

$$E_{\mathrm{CBM}}^{(SnO_2)_{(2)}/(TiO_2)_{(2)}} = E_{\mathrm{VBM}}^{(SnO_2)_{(2)}/(TiO_2)_{(2)}} - E_g \quad (3)$$

For the $(SnO_2)_{(3)}/(TiO_2)_{(3)}$ superlattice :

$$E_{\mathrm{VBM}}^{(SnO_2)_{(3)}/(TiO_2)_{(3)}} = \left((\chi_{\mathrm{Sn}}^3\chi_{\mathrm{Ti}}^3\chi_{\mathrm{O}}^{12})^{\frac{1}{18}}\right) - E_0 + \frac{1}{2}E_g \quad (4)$$

$$E_{\mathrm{CBM}}^{(SnO_2)_{(3)}/(TiO_2)_{(3)}} = E_{\mathrm{VBM}}^{(SnO_2)_{(3)}/(TiO_2)_{(3)}} - E_g \quad (5)$$

For the $(SnO_2)_{(1)}/(TiO_2)_{(2)}$ superlattice :

$$E_{\mathrm{VBM}}^{(SnO_2)_{(1)}/(TiO_2)_{(2)}} = \left((\chi_{\mathrm{Sn}}^1\chi_{\mathrm{Ti}}^2\chi_{\mathrm{O}}^6)^{\frac{1}{9}}\right) - E_0 + \frac{1}{2}E_g \quad (6)$$

$$E_{\mathrm{CBM}}^{(SnO_2)_{(1)}/(TiO_2)_{(2)}} = E_{\mathrm{VBM}}^{(SnO_2)_{(1)}/(TiO_2)_{(2)}} - E_g \quad (7)$$

*Corresponding author. Email: najwa.harrati@univ-artois.fr
†Corresponding author. Email: adlane.sayede@univ-artois.fr

For the $(SnO_2)_{(1)}/(TiO_2)_{(3)}$ superlattice :

$$E_{\mathrm{VBM}}^{(SnO_2)_{(1)}/(TiO_2)_{(3)}} = \left((\chi_{\mathrm{Sn}}^{1}\chi_{\mathrm{Ti}}^{3}\chi_{\mathrm{O}}^{8})^{\frac{1}{12}}\right) - E_0 + \frac{1}{2}E_g \tag{8}$$

$$E_{\mathrm{CBM}}^{(SnO_2)_{(1)}/(TiO_2)_{(3)}} = E_{\mathrm{VBM}}^{(SnO_2)_{(1)}/(TiO_2)_{(3)}} - E_g \tag{9}$$

For the $(SnO_2)_{(2)}/(TiO_2)_{(1)}$ superlattice :

$$E_{\mathrm{VBM}}^{(SnO_2)_{(2)}/(TiO_2)_{(1)}} = \left((\chi_{\mathrm{Sn}}^{2}\chi_{\mathrm{Ti}}^{1}\chi_{\mathrm{O}}^{6})^{\frac{1}{9}}\right) - E_0 + \frac{1}{2}E_g \tag{10}$$

$$E_{\mathrm{CBM}}^{(SnO_2)_{(2)}/(TiO_2)_{(1)}} = E_{\mathrm{VBM}}^{(SnO_2)_{(2)}/(TiO_2)_{(1)}} - E_g \tag{11}$$

Supplementary Tables

Table S1: Calculated lattice parameters for the tetragonal phases of SnO_2 and TiO_2 in this work, compared with the experimental data.

Lattice parameters (Å)		a	c
SnO_2	This work	4.737	3.211
	Experimental [1]	4.737	3.187
TiO_2	This work	4.591	2.951
	Experimental [2]	4.593	2.958

Table S2: Average bond lengths d(Sn-O) (Å) under compressive and tensile strains of nSO/mTO superlattices.

	1SO/1TO	2SO/2TO	3SO/3TO	1SO/2TO	1SO/3TO	2SO/1TO	3SO/1TO
-5%	2.11042	2.17630	2.19501	2.12215	2.12803	2.16830	2.11062
-4%	2.11024	2.15318	2.15300	2.11417	2.12329	2.14615	2.10692
-3%	2.11000	2.13563	2.13468	2.11125	2.11409	2.13063	2.10332
-2%	2.10151	2.11970	2.11885	2.09610	2.09574	2.11606	2.10022
-1%	2.08769	2.10572	2.10527	2.08114	2.07873	2.10297	2.09737
0%	2.07293	2.09264	2.09217	2.06552	2.06209	2.08958	2.09474
1%	2.05899	2.08121	2.08049	2.05094	2.04794	2.07856	2.09284
2%	2.04511	2.06991	2.06916	2.03629	2.03133	2.06750	2.09162
3%	2.03302	2.06108	2.06020	2.02337	2.01540	2.05905	2.09108
4%	2.02117	2.05343	2.05172	2.01940	2.00585	2.05047	2.09077
5%	2.00855	2.04703	2.04409	1.99492	2.00428	2.04515	2.09000

Table S3: Average bond lenghts d(Ti-O) (Å) under compressive and tensile strains of nSO/mTO superlattices.

	1SO/1TO	2SO/2TO	3SO/3TO	1SO/2TO	1SO/3TO	2SO/1TO	3SO/1TO
-5%	2.16233	2.04482	2.07104	2.10161	2.09922	2.13906	2.00921
-4%	2.08691	2.02875	2.02625	2.04987	2.04652	2.06495	2.00614
-3%	2.05776	2.01533	2.01082	2.02770	2.02208	2.04320	2.00363
-2%	2.03899	2.00239	1.99845	2.01249	2.00484	2.02659	2.00043
-1%	2.02436	1.99048	1.98778	2.00057	1.99141	2.01257	1.99843
0%	2.01020	1.97906	1.97761	1.98887	1.98038	1.99848	1.99670
1%	1.99815	1.96870	1.96900	1.97933	1.97330	1.98695	1.97488
2%	1.98653	1.95847	1.96087	1.97224	1.96781	1.97528	1.96436
3%	1.97820	1.95040	1.95571	1.96942	1.96490	1.96743	1.95404
4%	1.97192	1.94357	1.95259	1.96941	1.94624	1.96044	1.94444
5%	1.97060	1.93794	1.95202	1.95330	1.93649	1.95286	1.93488

Table S4: The calculated optimal strain and energy of nSO/mTO superlattices in response to biaxial tensile and compressive strains.

Superlattices	Strain opt.(%)	Energy opt. (eV)
1SO/1TO	0.35	-90.5182
2SO/2TO	0.40	-181.4230
3SO/3TO	0.41	-272.3470
1SO/2TO	0.25	-144.2511
1SO/3TO	0.20	-197.9337
2SO/1TO	0.58	-127.7512
3SO/1TO	2.57	-165.1628

Table S5: The calculated elastic constants C_{ij} (in GPa) of unstrained nSO/mTO superlattices.

$\varepsilon = 0\%$	C_{11}	C_{33}	C_{44}	C_{66}	C_{12}	C_{13}
1SO/1TO	254.608	365.642	110.598	192.575	142.330	125.041
2SO/2TO	264.250	385.436	103.106	198.899	151.257	133.075
3SO/3TO	259.135	384.173	96.976	198.865	146.727	126.153
1SO/2TO	272.277	413.527	112.847	198.058	154.466	138.412
1SO/3TO	279.915	427.779	84.391	199.936	159.623	140.802
2SO/1TO	246.701	339.427	103.649	188.416	138.674	116.879
3SO/1TO	239.334	332.293	99.367	187.272	134.221	113.702

Table S6: The calculated Bulk Modulus (B), Shear Modulus (G), $\frac{B}{G}$ ratio, Young's modulus (E), Poisson's ratio (ν) and Debye temperature (θ_{D}) of unstrained nSO/mTO superlattices.

$\varepsilon = 0\%$	B (GPa)	G (GPa)	$\frac{B}{G}$	E (GPa)	ν	θ_{D}(K)
1SO/1TO	183.145	107.492	1.70	269.709	0.255	644.6
2SO/2TO	192.485	106.167	1.81	269.038	0.267	641.1
3SO/3TO	186.721	102.765	1.82	260.504	0.267	630.7
1SO/2TO	199.844	110.308	1.81	279.500	0.267	687.6
1SO/3TO	205.007	104.101	1.97	267.094	0.283	687.8
2SO/1TO	174.433	103.072	1.69	258.333	0.253	602.7
3SO/1TO	169.480	101.235	1.67	253.276	0.251	584.6

Table S7: CBMs and VBMs (eV) of nSO/mTO superlattices with (n=m) stacking periodicity under biaxial strains effect.

Strain	1SO/1TO		2SO/2TO		3SO/3TO	
	CBMs	VBMs	CBMs	VBMs	CBMs	VBMs
(%)	(eV)	(eV)	(eV)	(eV)	(eV)	(eV)
-3	7.966	4.632	8.019	4.750	7.914	4.748
-2	7.866	4.457	7.931	4.555	7.801	4.550
-1	7.755	4.303	7.830	4.392	7.659	4.376
0	7.611	4.155	7.661	4.228	7.455	4.202
1	7.456	4.027	7.412	4.087	7.213	4.049
2	7.272	3.898	7.121	3.949	6.919	3.902
3	7.097	3.785	6.848	3.829	6.626	3.781
4	6.669	3.513	6.211	3.558	5.929	3.569

Table S8: CBMs and VBMs of nSO/mTO superlattices with (1, m) stacking periodicity under biaxial strains effect.

Strain	1SO/2TO		1SO/3TO	
	CBMs	VBMs	CBMs	VBMs
(%)	(eV)	(eV)	(eV)	(eV)
-3	7.769	4.497	7.594	4.402
-2	7.684	4.310	7.498	4.231
-1	7.638	4.171	7.399	4.079
0	7.432	3.983	7.257	3.922
1	7.203	3.841	7.004	3.782
2	6.911	3.694	6.688	3.678
3	6.644	3.567	6.404	3.607
4	6.105	3.344	5.851	3.314

Table S9: CBMs and VBMs of nSO/mTO superlattices with (n,1) stacking periodicity under biaxial strains effect .

Strain	2SO/1TO		3SO/1TO	
	CBMs	VBMs	CBMs	VBMs
(%)	(eV)	(eV)	(eV)	(eV)
-5			8.909	5.130
-4			8.649	5.010
-3	8.286	4.873	8.403	4.886
-2	8.203	4.688	8.159	4.759
-1	8.096	4.530	7.932	4.629
0	7.912	4.380	7.690	4.482
1	7.663	4.245	7.462	4.336
2	7.376	4.109	7.216	4.172
3	7.101	3.992	6.999	4.023
4	5.693	3.359	6.774	3.862
5			6.540	3.692

Supplementary Figures

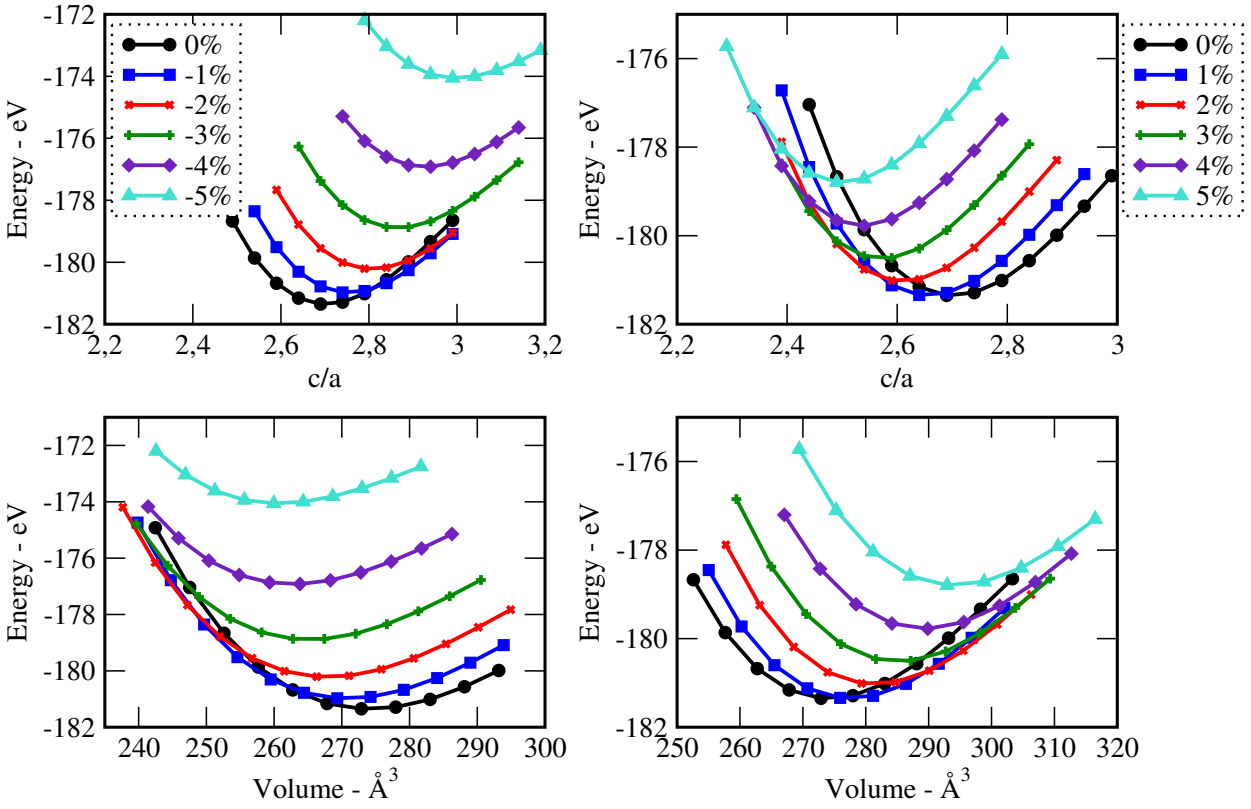

(a) 2:2

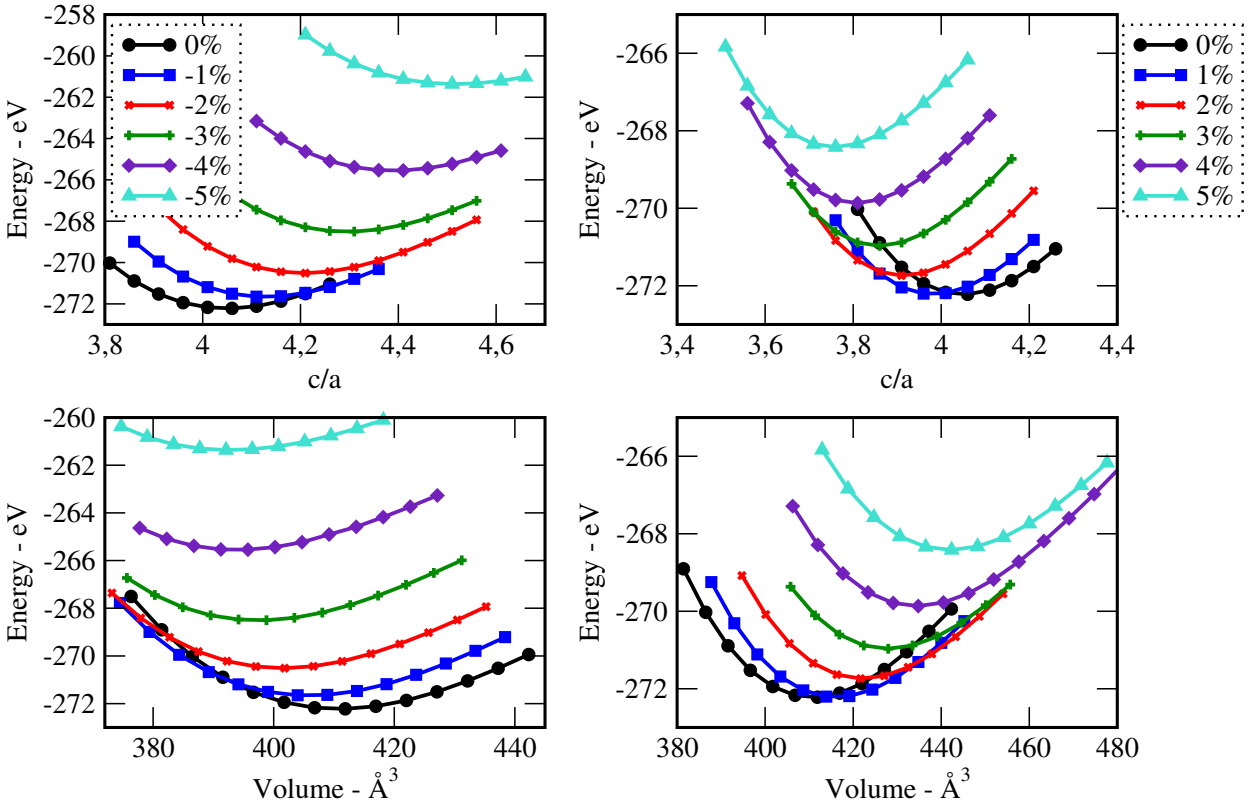

(b) 3:3

Figure S1: Structure stability of (a) 2SO/2TO and (b) 3SO/3TO superlattices under compressive (left) and tensile (right) strains.

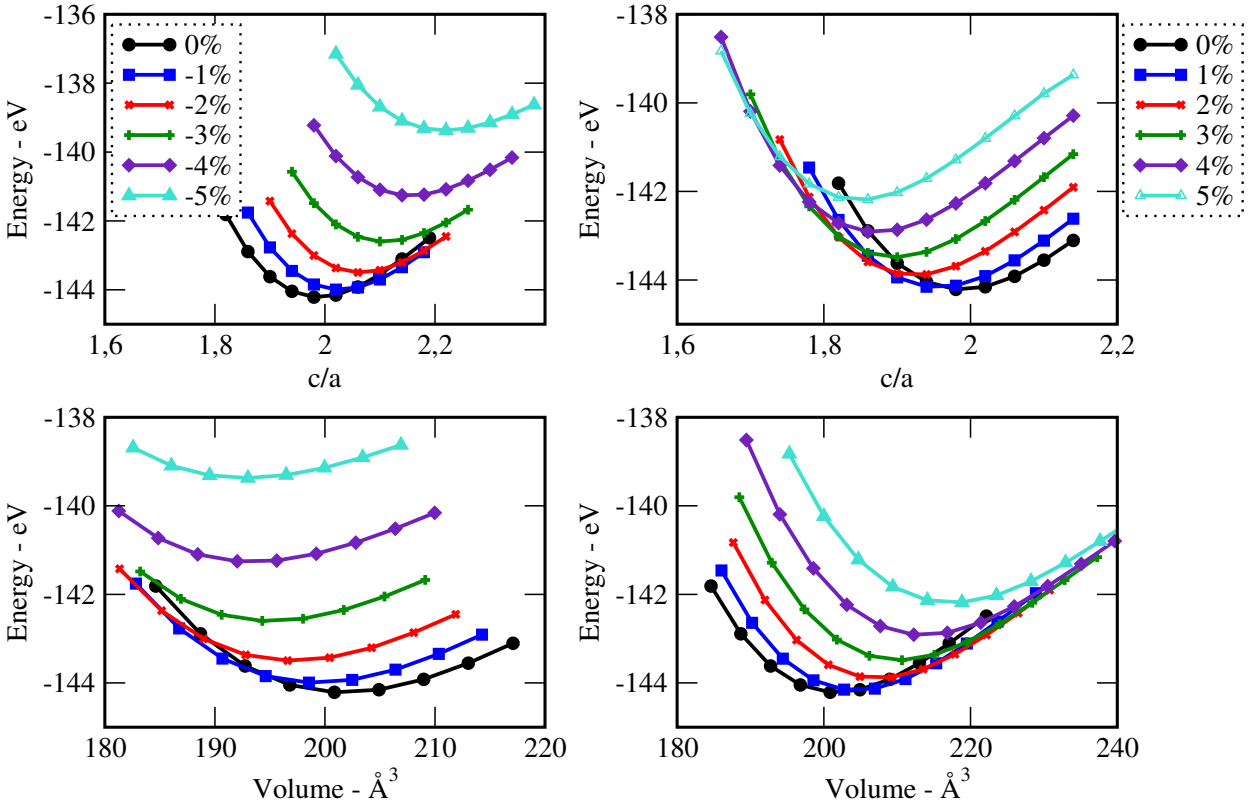

(a) 1:2

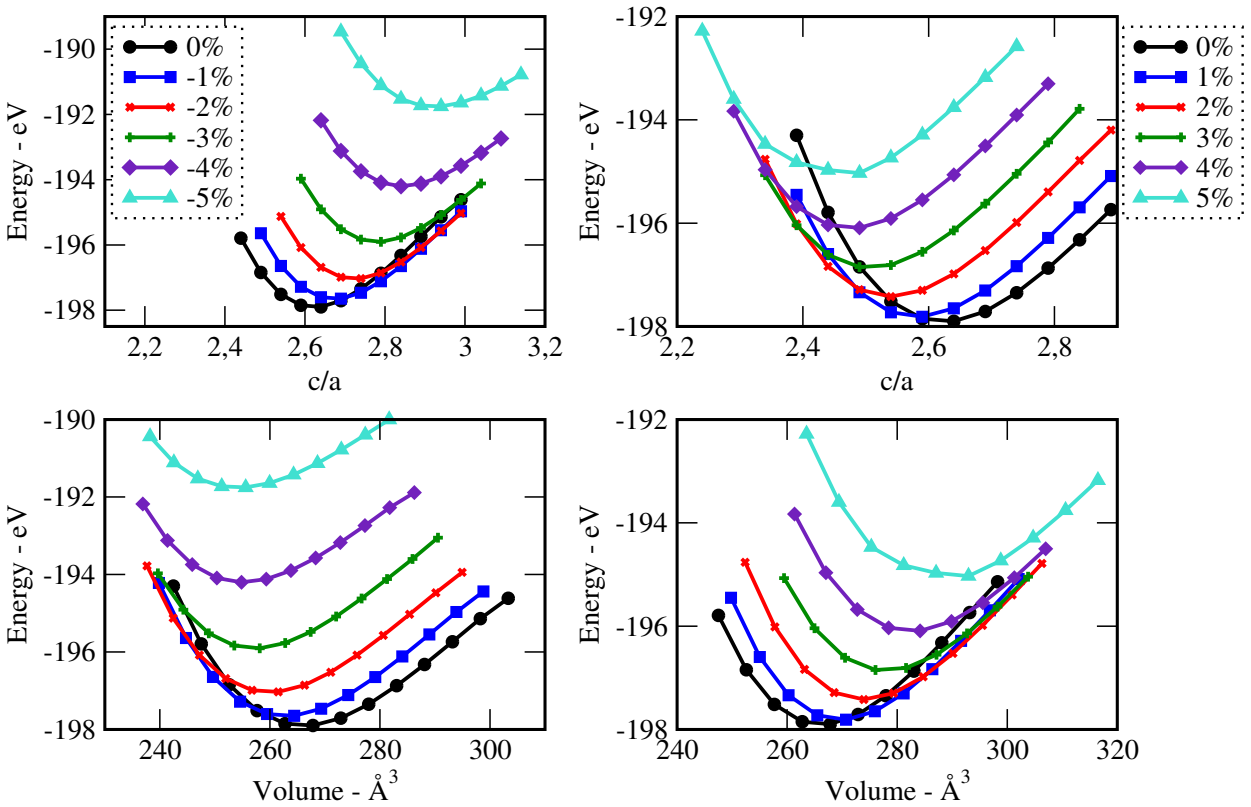

(b) 1:3

Figure S2: Structure stability of (a) 1SO/2TO and (b) 1SO/3TO superlattices under compressive (left) and tensile (right) strains.

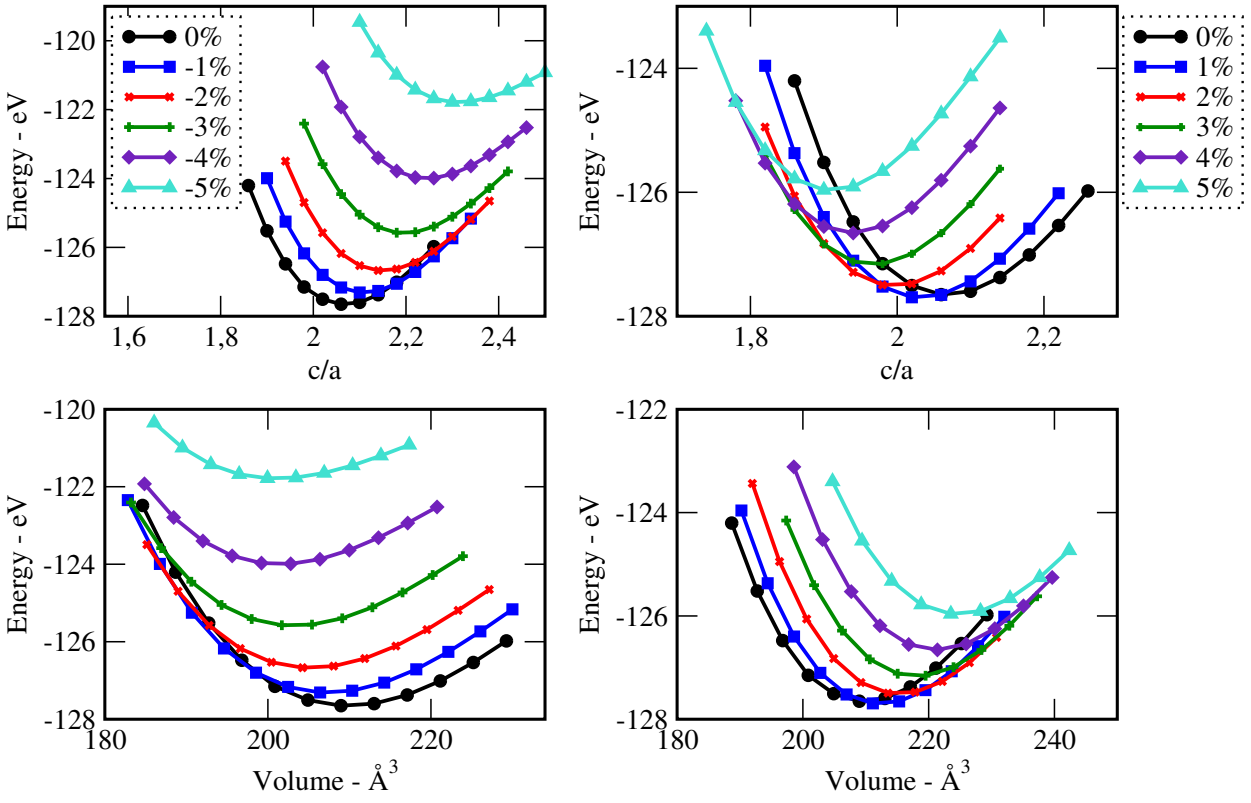

(a) 2:1

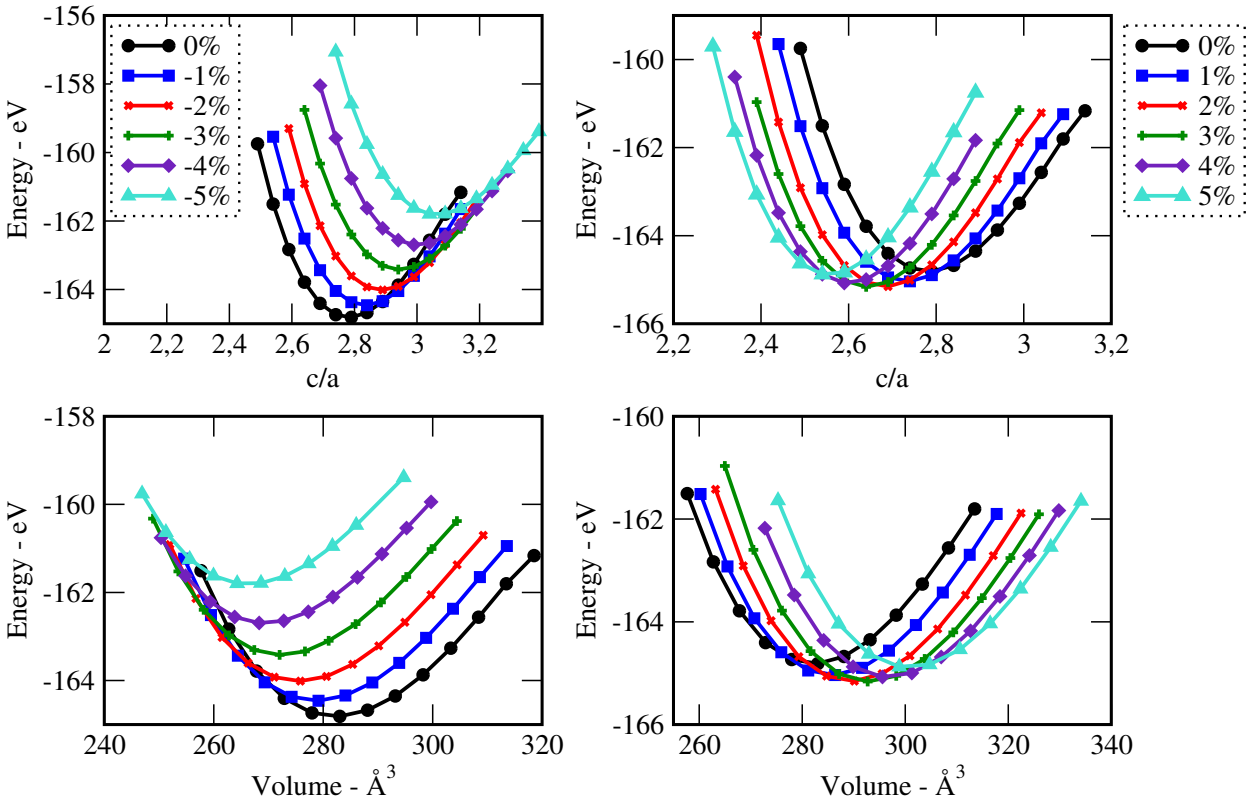

(b) 3:1

Figure S3: Structure stability of (a) 2SO/1TO and (b) 3SO/1TO superlattices under compressive (left) and tensile (right) strains..

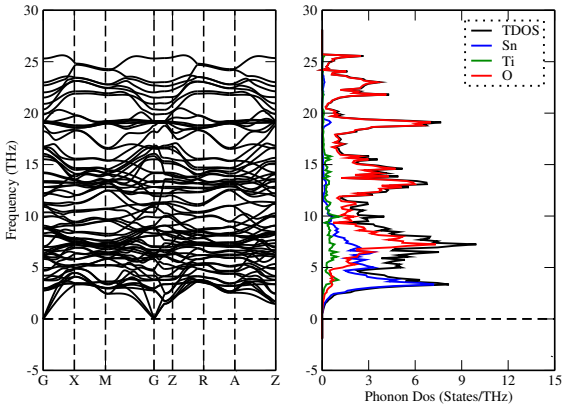

(a) -4%

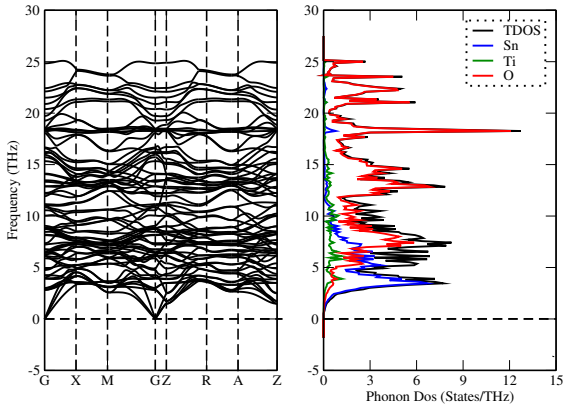

(b) -3%

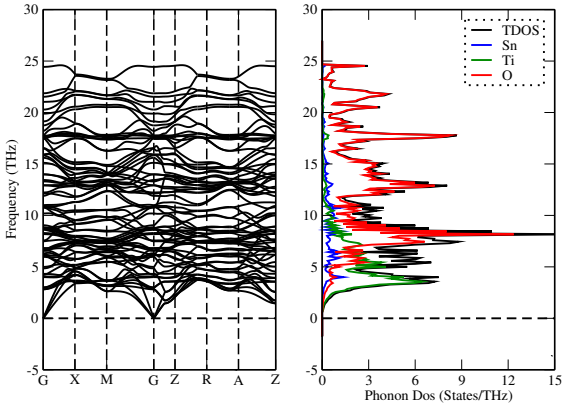

(c) -2%

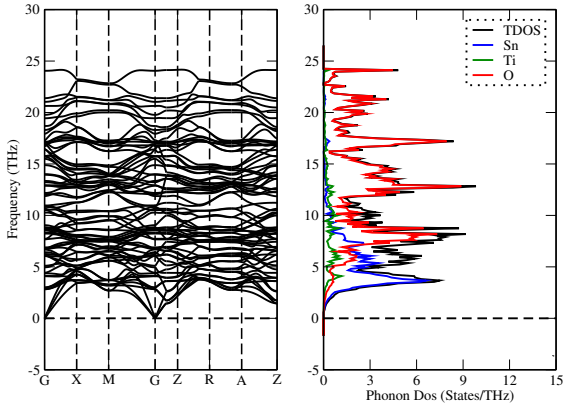

(d) -1%

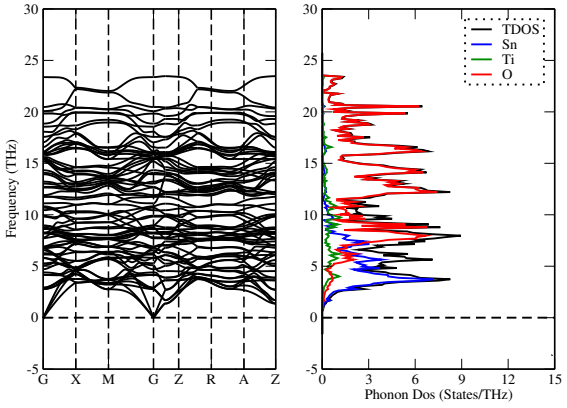

(e) 1%

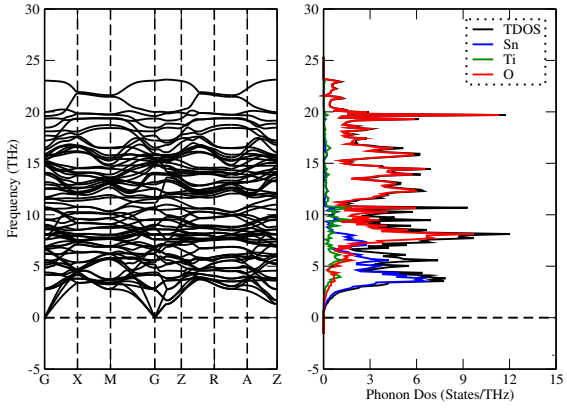

(f) 2%

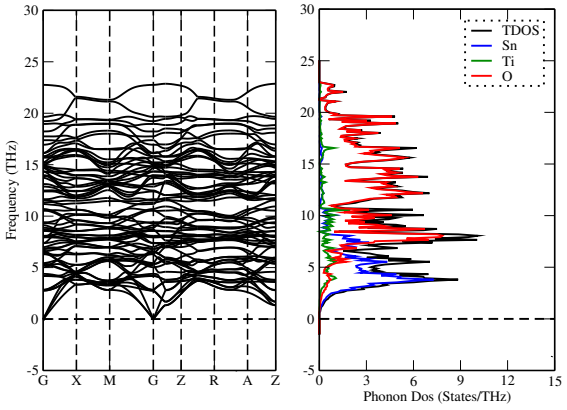

(g) 3%

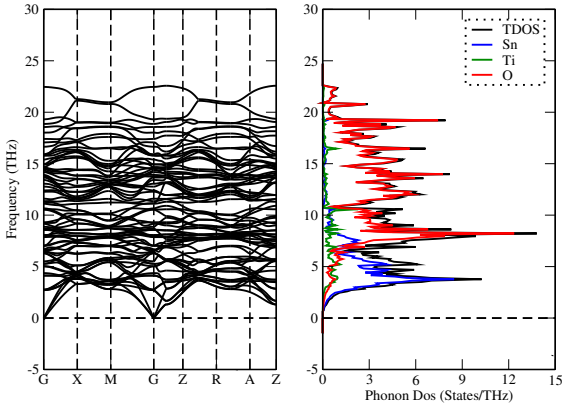

(h) 4%

Figure S4: (a-h) Phonon dispersion curves and phonon densities of states of strained 3SO/1TO superlattice under different biaxial compressive (-4%, -3%, -2%, and -1%) and tensile (1%, 2%, 3%, and 4%) strains.

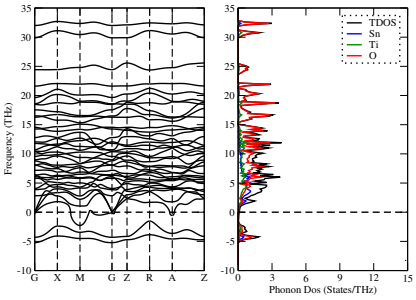

(a) -5%

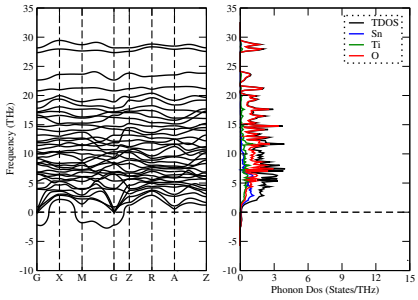

(b) -4%

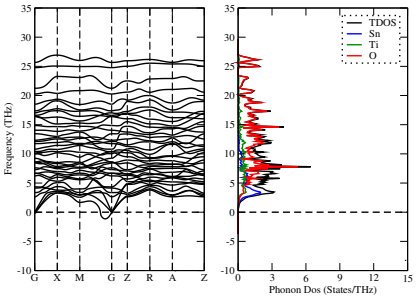

(c) -3%

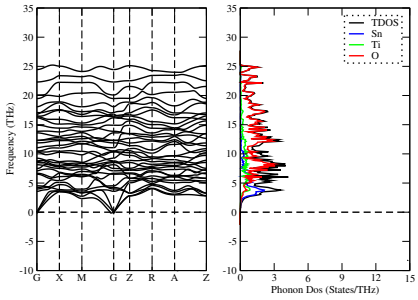

(d) -2%

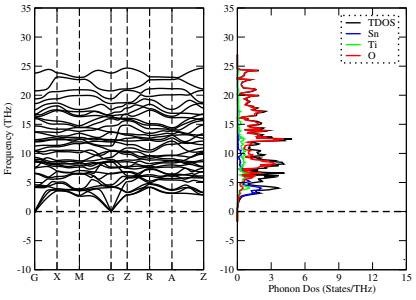

(e) -1%

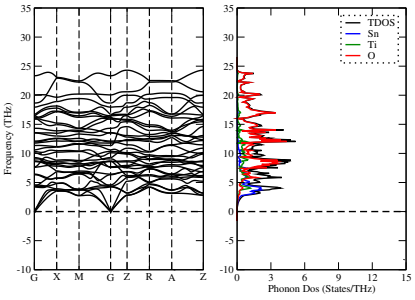

(f) 0%

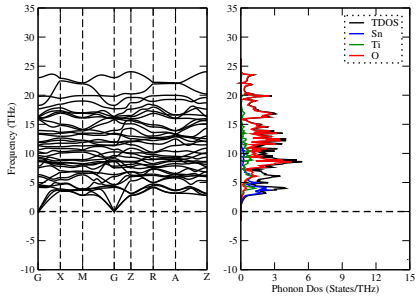

(g) 1%

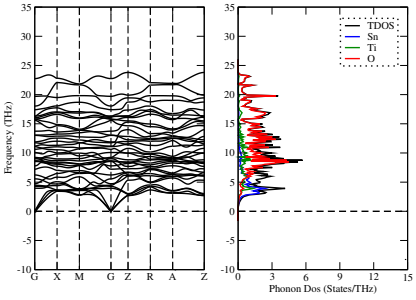

(h) 2%

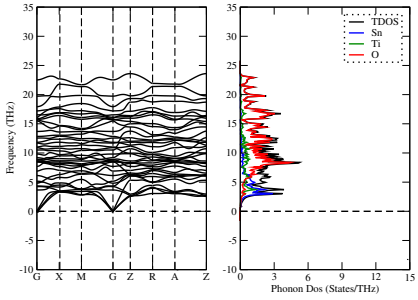

(i) 3%

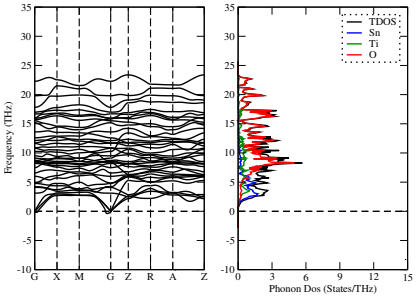

(j) 4%

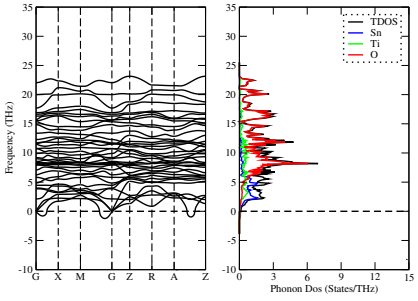

(k) 5%

Figure S5: (a-k) Phonon dispersion curves and phonon densities of states of unstrained and strained 1SO/1TO superlattice under different biaxial compressive (-5%, -4%, -3%, -2%, and -1%) and tensile (1%, 2%, 3%, 4%, and 5%) strains.

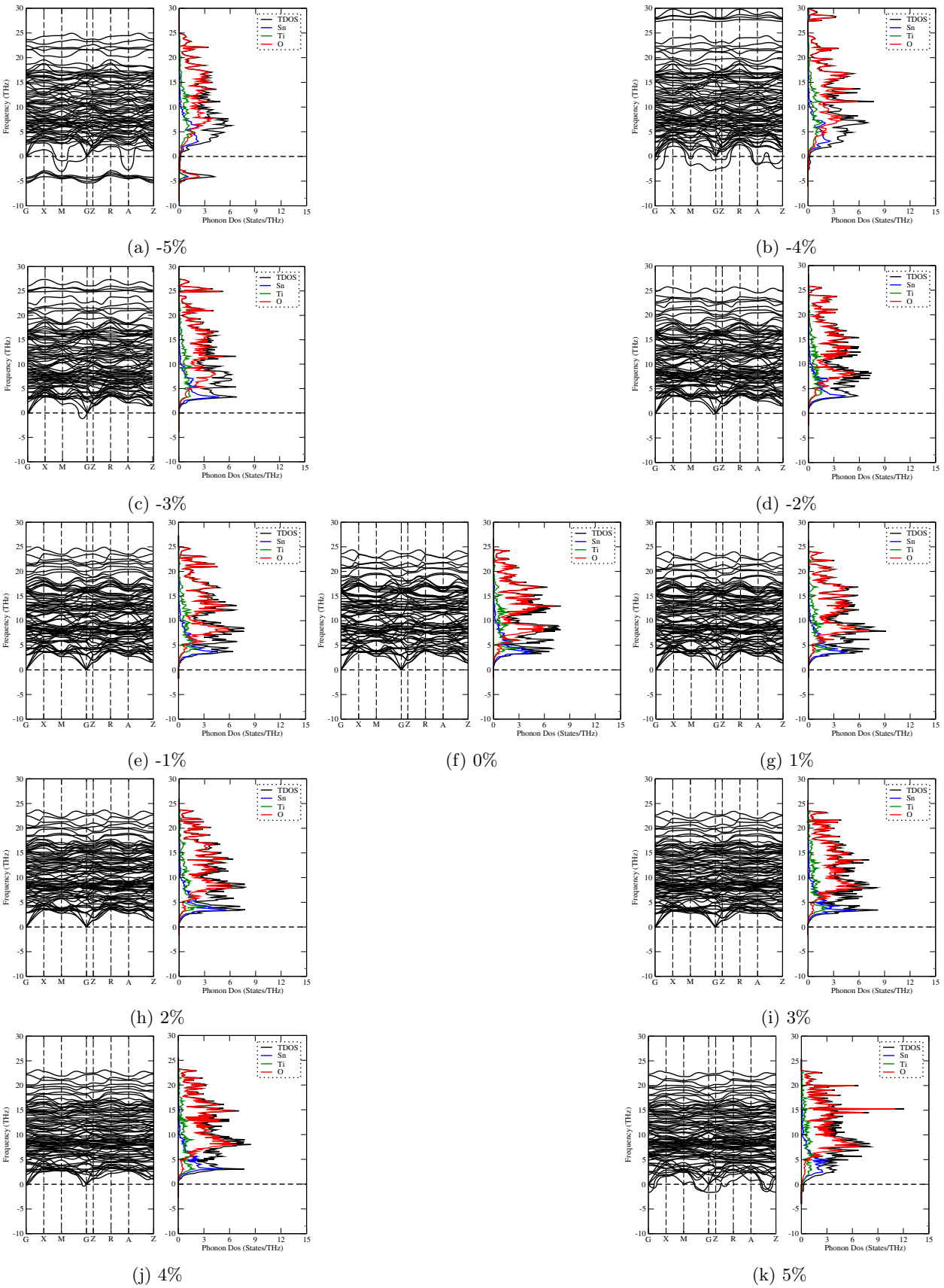

(a) -5% (b) -4%

(c) -3% (d) -2%

(e) -1% (f) 0% (g) 1%

(h) 2% (i) 3%

(j) 4% (k) 5%

Figure S6: (a-k) Phonon dispersion curves and phonon densities of states of unstrained and strained 2SO/2TO superlattice under different biaxial compressive (-5%, -4%, -3%, -2%, and -1%) and tensile (1%, 2%, 3%, 4%, and 5%) strains.

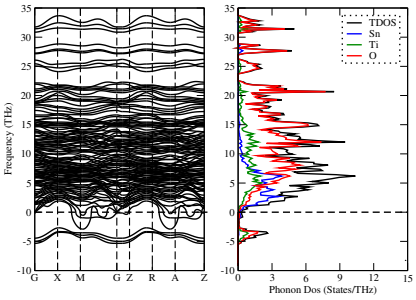

(a) -5%

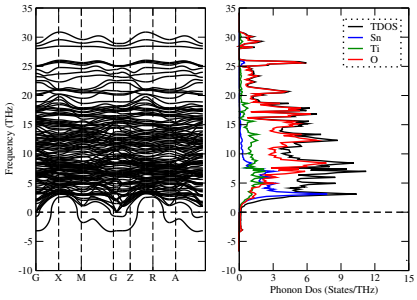

(b) -4%

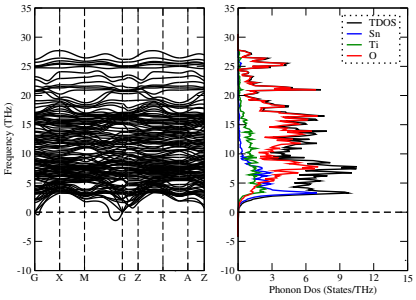

(c) -3%

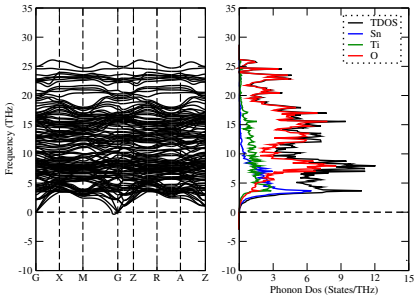

(d) -2%

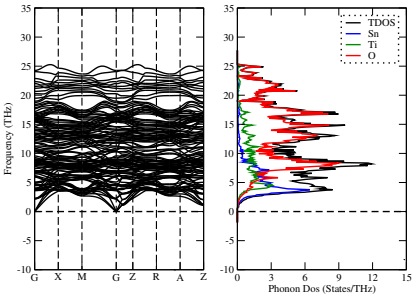

(e) -1%

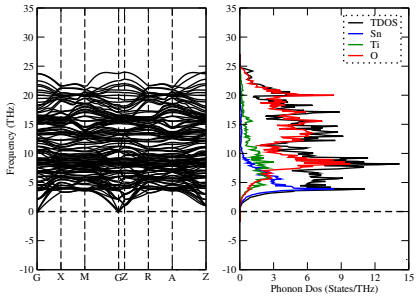

(f) 0%

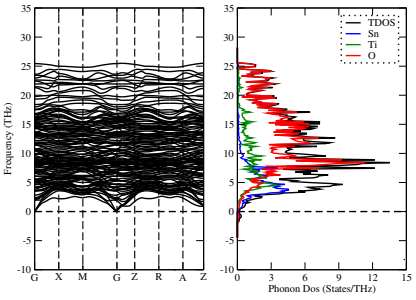

(g) 1%

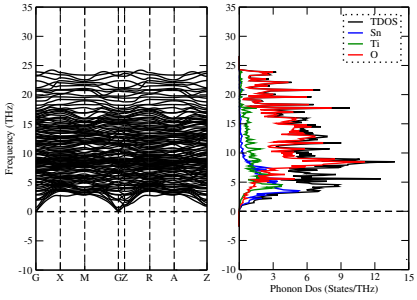

(h) 2%

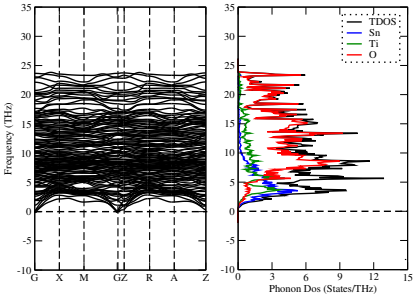

(i) 3%

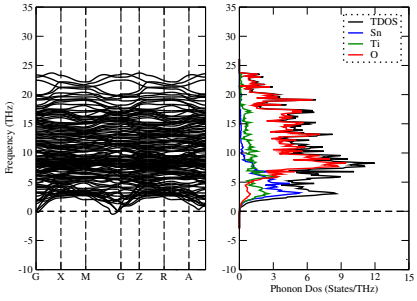

(j) 4%

Figure S7: (a-k) Phonon dispersion curves and phonon densities of states of unstrained and strained 3SO/3TO superlattice under different biaxial compressive (-5%, -4%, -3%, -2%, and -1%) and tensile (1%, 2%, 3%, 4%, and 5%) strains.

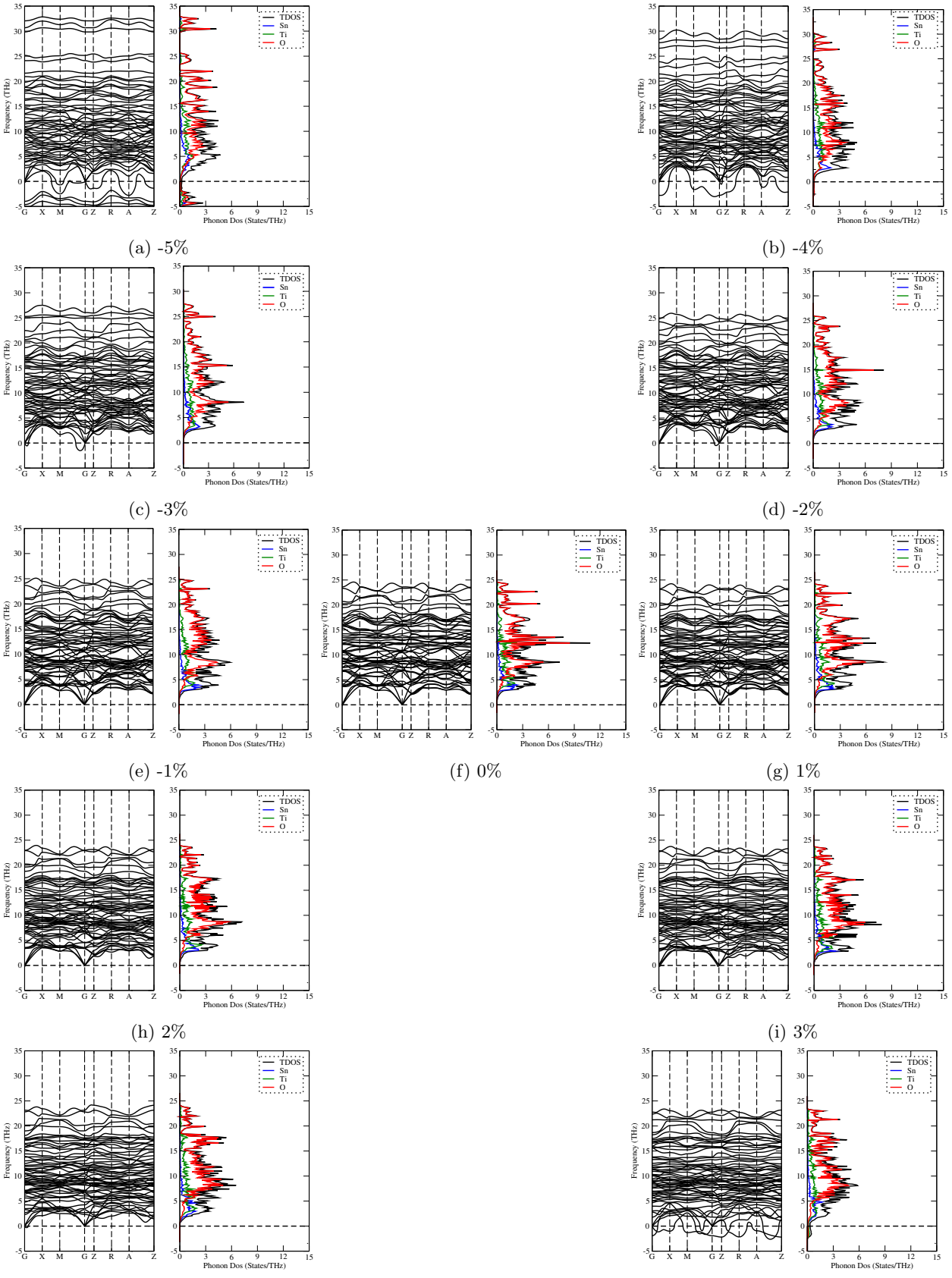

(a) -5% (b) -4%

(c) -3% (d) -2%

(e) -1% (f) 0% (g) 1%

(h) 2% (i) 3%

(j) 4% (k) 5%

Figure 8: (a-k) Phonon dispersion curves and phonon densities of states of unstrained and strained 1SO/2TO superlattice under different biaxial compressive (-5%, -4%, -3%, -2%, and -1%) and tensile (1%, 2%, 3%, 4%, and 5%) strains.

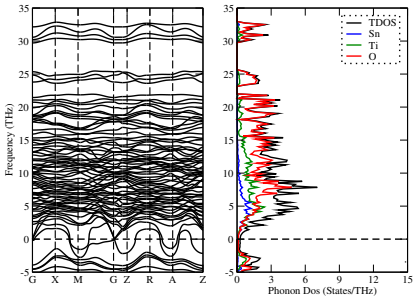

(a) -5%

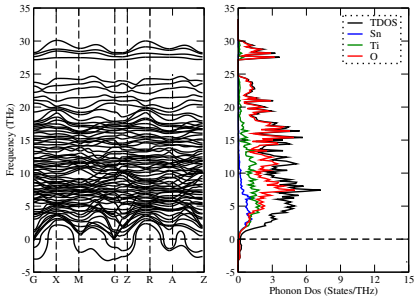

(b) -4%

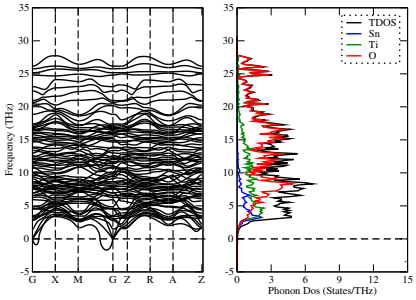

(c) -3%

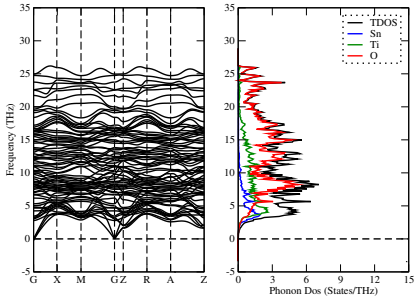

(d) -2%

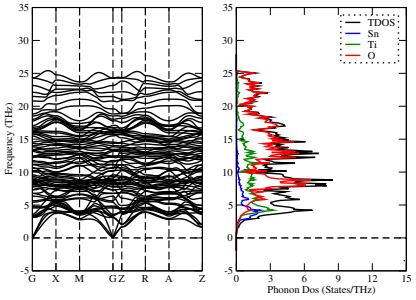

(e) -1%

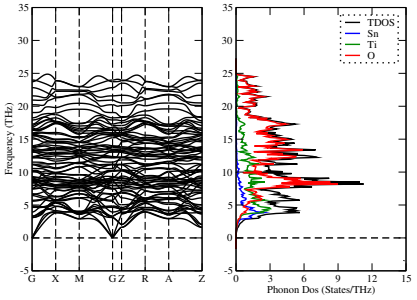

(f) 0%

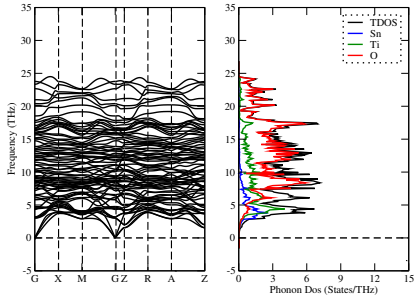

(g) 1%

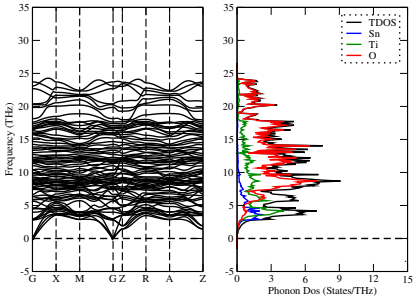

(h) 2%

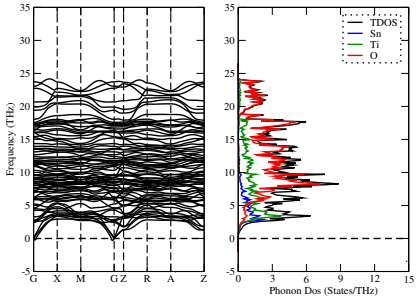

(i) 3%

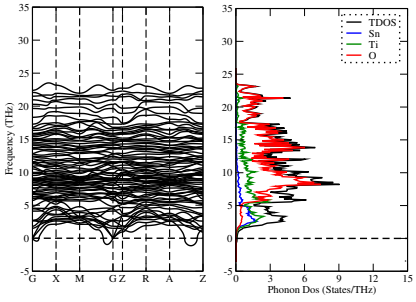

(j) 4%

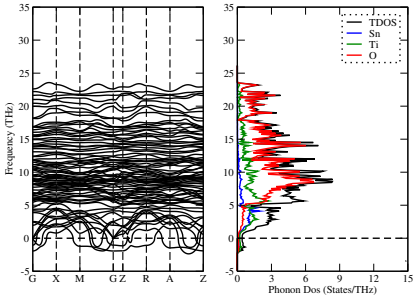

(k) 5%

Figure S9: (a-k) Phonon dispersion curves and phonon densities of states of unstrained and strained 1SO/3TO superlattice under different biaxial compressive (-5%, -4%, -3%, -2%, and -1%) and tensile (1%, 2%, 3%, 4%, and 5%) strains.

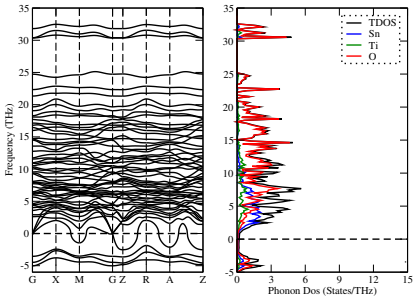

(a) -5%

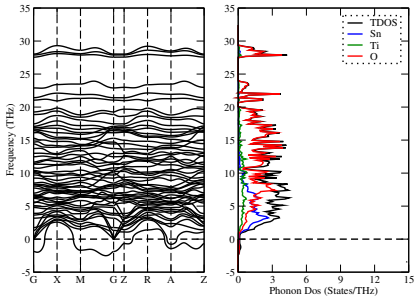

(b) -4%

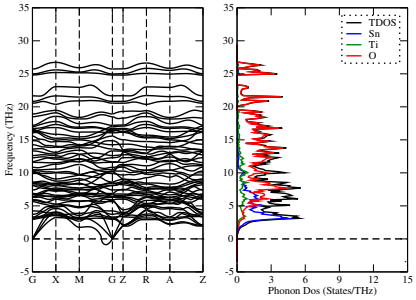

(c) -3%

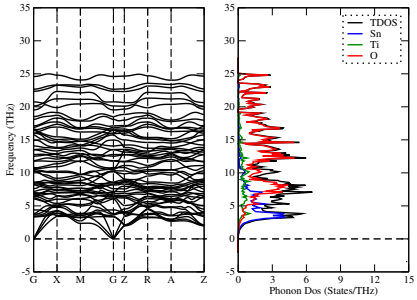

(d) -2%

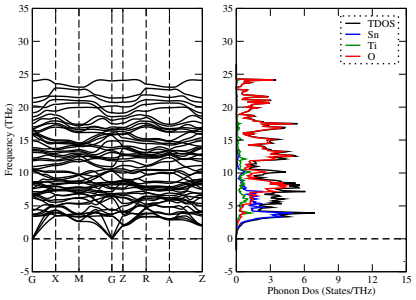

(e) -1%

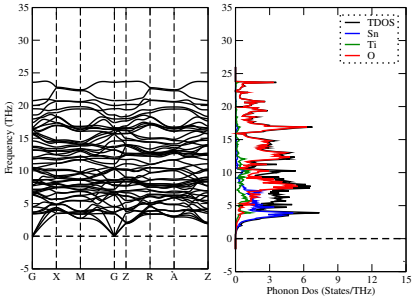

(f) 0%

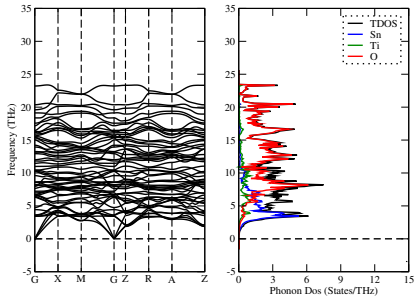

(g) 1%

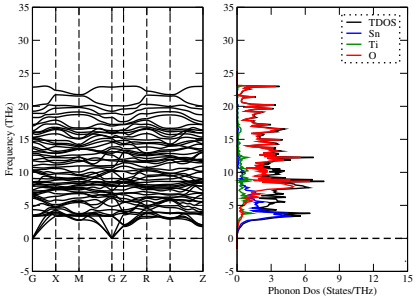

(h) 2%

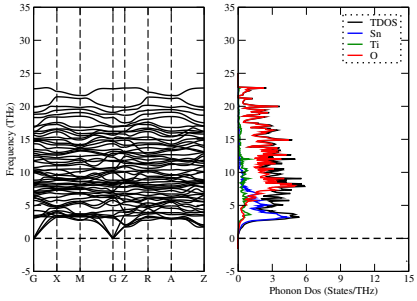

(i) 3%

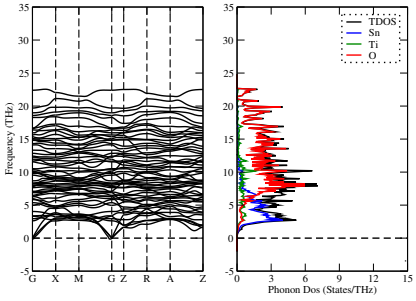

(j) 4%

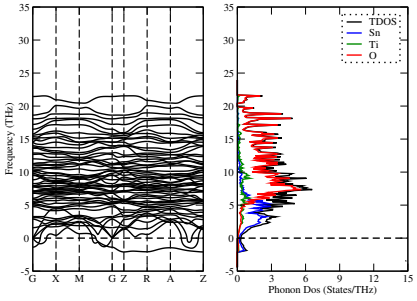

(k) 5%

Figure S10: (a-k) Phonon dispersion curves and phonon densities of states of unstrained and strained 2SO/1TO superlattice under different biaxial compressive (-5%, -4%, -3%, -2%, and -1%) and tensile (1%, 2%, 3%, 4%, and 5%) strains.

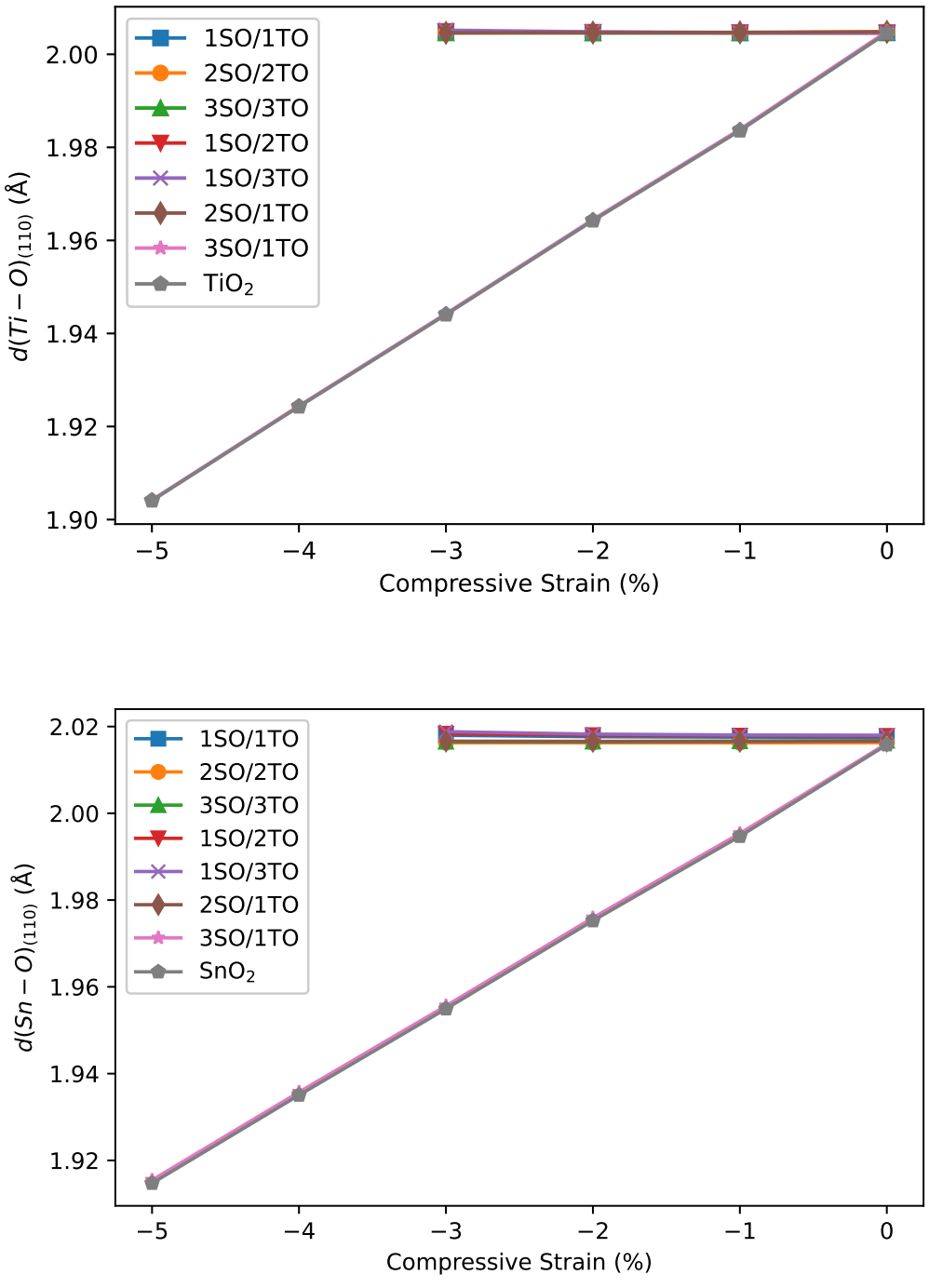

Figure S11: Bond lengths d(Ti-O) (upper part) and d(Sn-O) (bottom part) along (110) plane of nSO/mTO superlattices as a function of compressive strains.

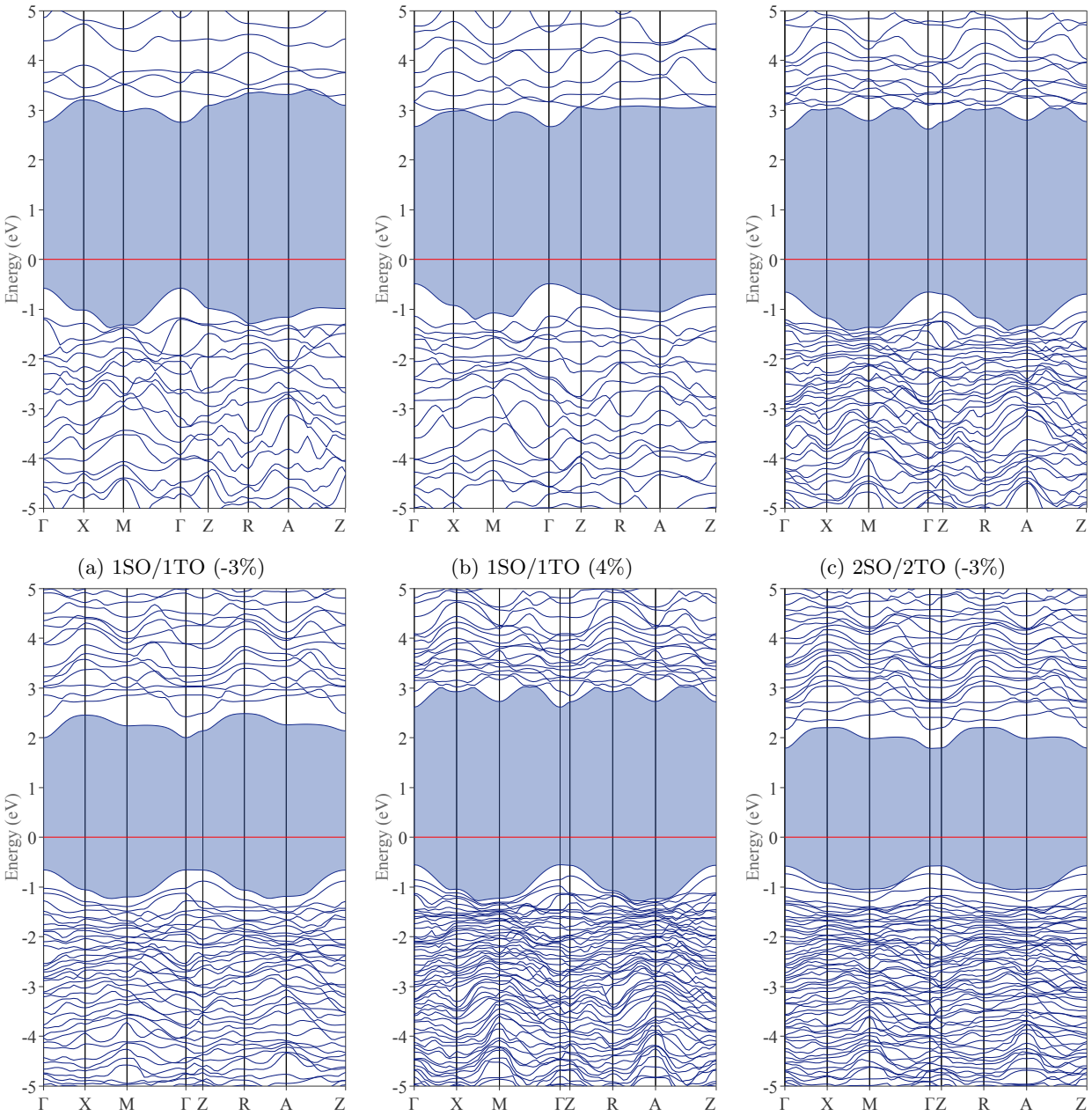

(a) 1SO/1TO (-3%) (b) 1SO/1TO (4%) (c) 2SO/2TO (-3%)

(d) 2SO/2TO (4%) (e) 3SO/3TO (-3%) (f) 3SO/3TO (4%)

Figure S12: (a-f) Band strucures of nSO/mTO superlattices with (n=m) stacking peroidicity at the upper limits of compressive and tensile strain.

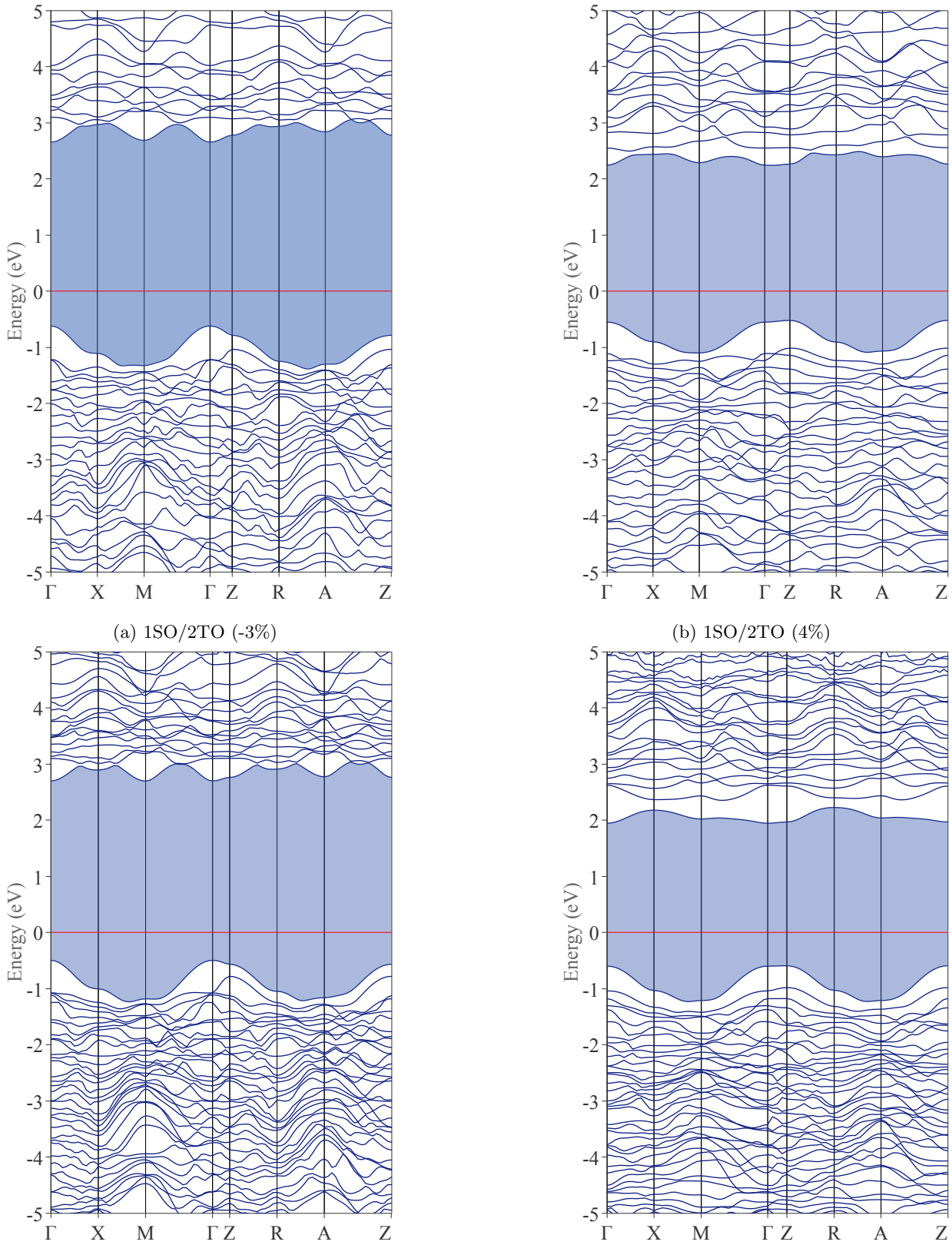

(a) 1SO/2TO (-3%)

(b) 1SO/2TO (4%)

(c) 1SO/3TO (-3%)

(d) 1SO/3TO (4%)

Figure S13: (a-d) Band strucures of nSO/mTO superlattices with (1, m) stacking peroidicity at the upper limits of compressive and tensile strain.

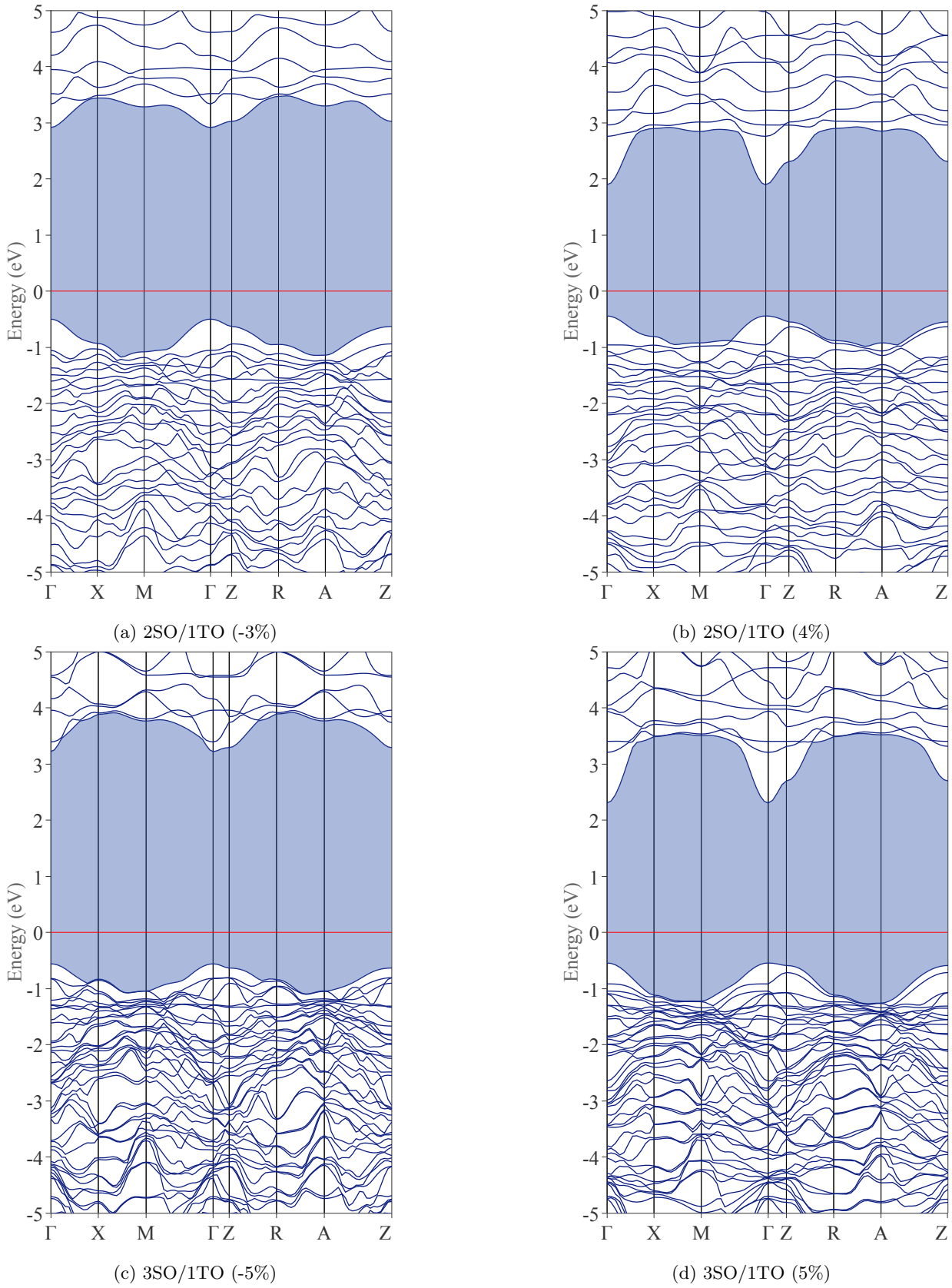

(a) 2SO/1TO (-3%)

(b) 2SO/1TO (4%)

(c) 3SO/1TO (-5%)

(d) 3SO/1TO (5%)

Figure S14: (a-d) Band strucures of nSO/mTO superlattices with (n, 1) stacking peroidicity at the upper limits of compressive and tensile strain.

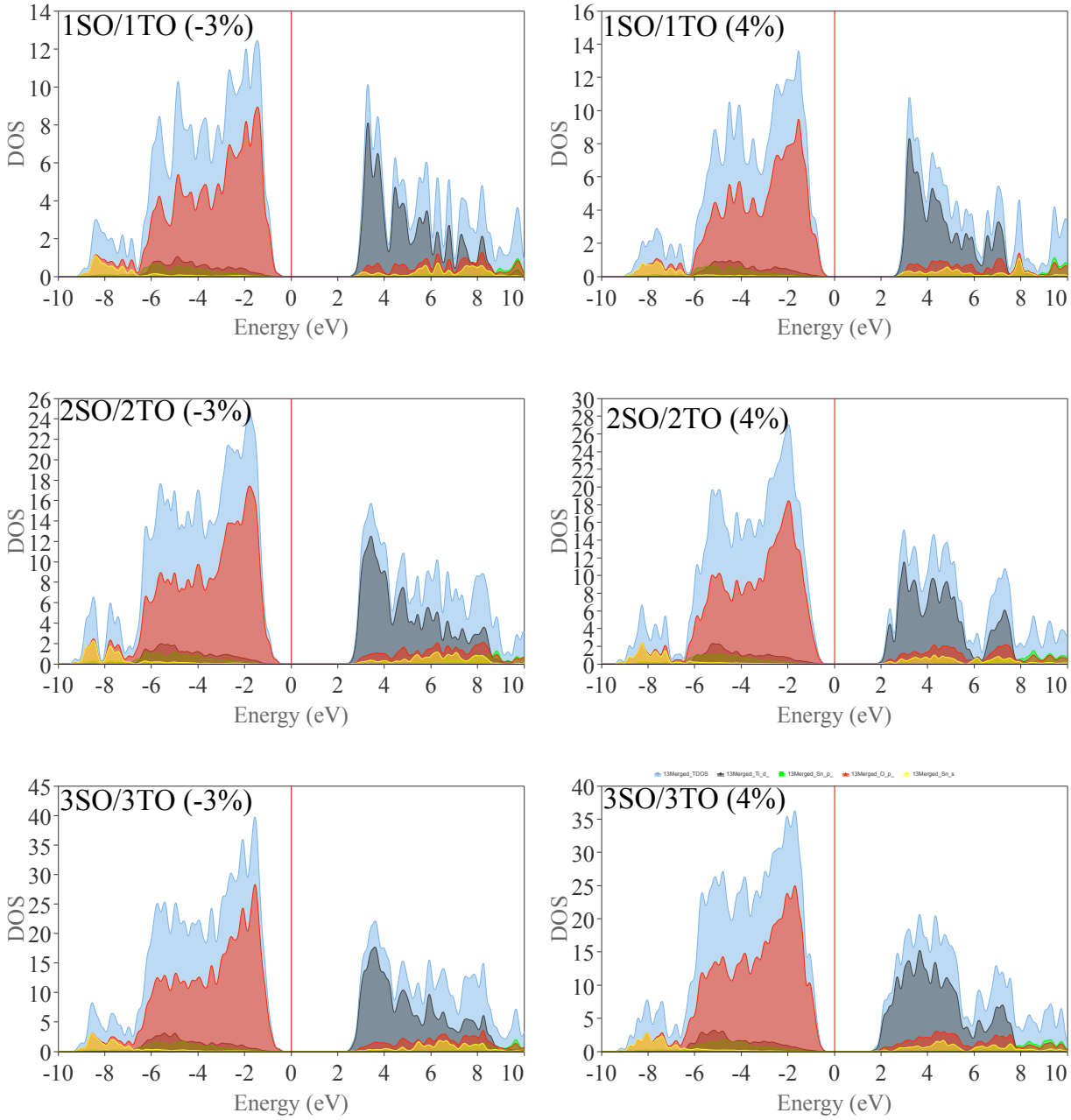

Figure 15: Total and Projected Density of states of nSO/mTO superlattices with (n = m) stacking peroidicity at the upper limits of compressive and tensile strain. The Fermi level is located at zero (0 eV).

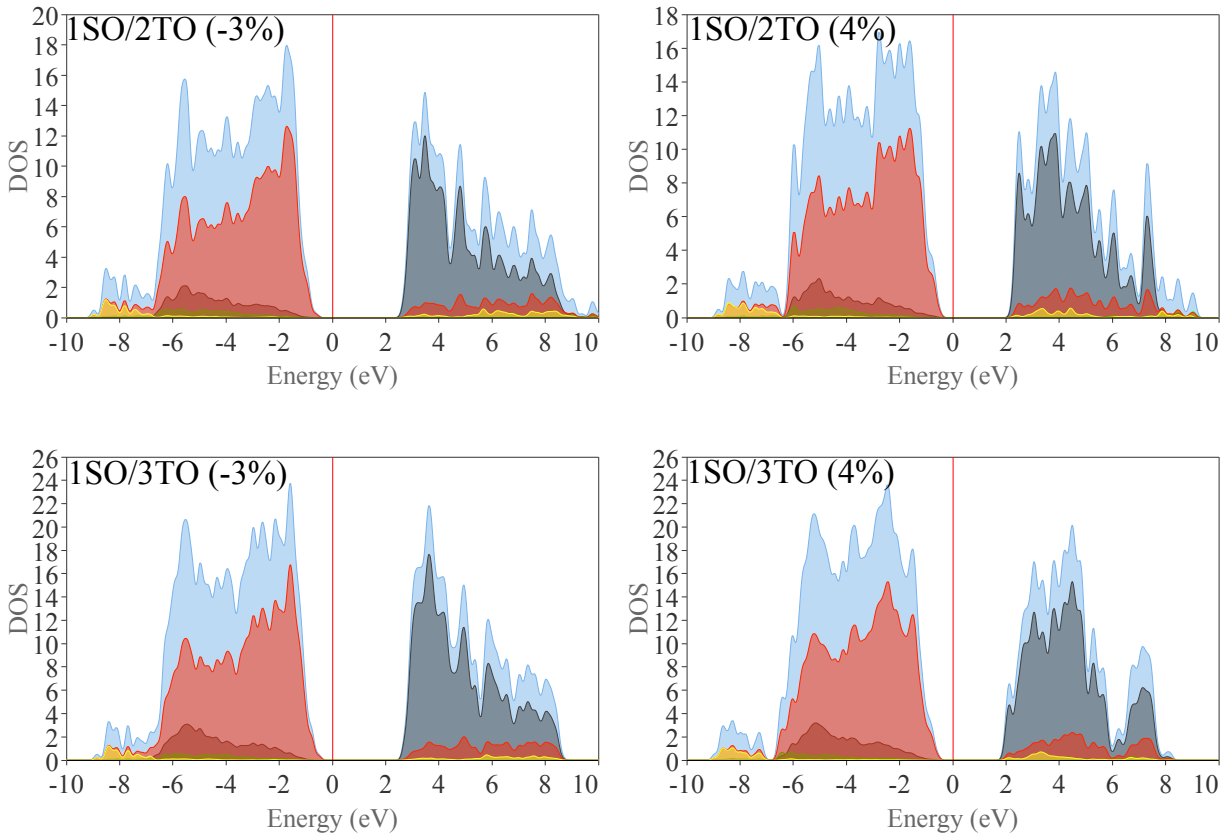

Figure 16: Total and Projected Density of states of nSO/mTO superlattices with (1, m) stacking peroidicity at the upper limits of compressive and tensile strain. The Fermi level is located at zero (0 eV).

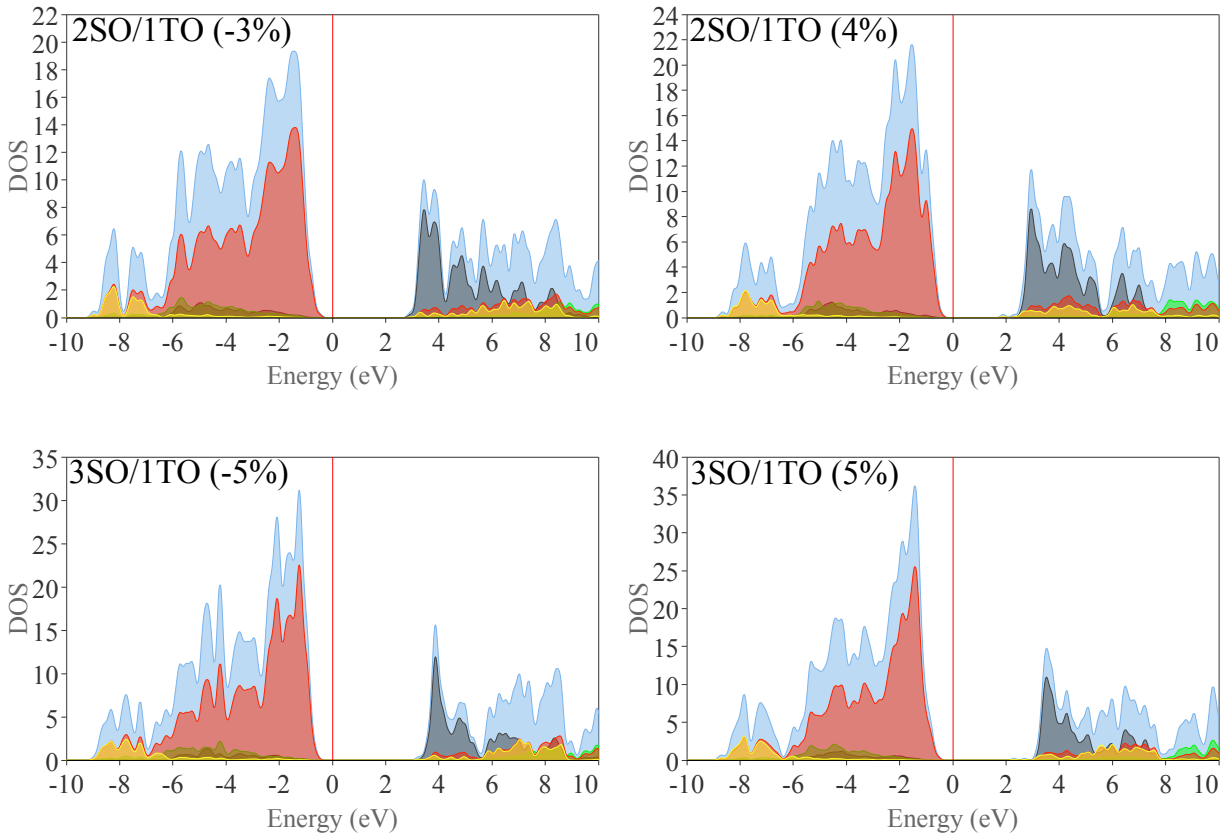

Figure 17: Total and Projected Density of states of nSO/mTO superlattices with (n, 1) stacking peroidicity at the upper limits of compressive and tensile strain. The Fermi level is located at zero (0 eV).

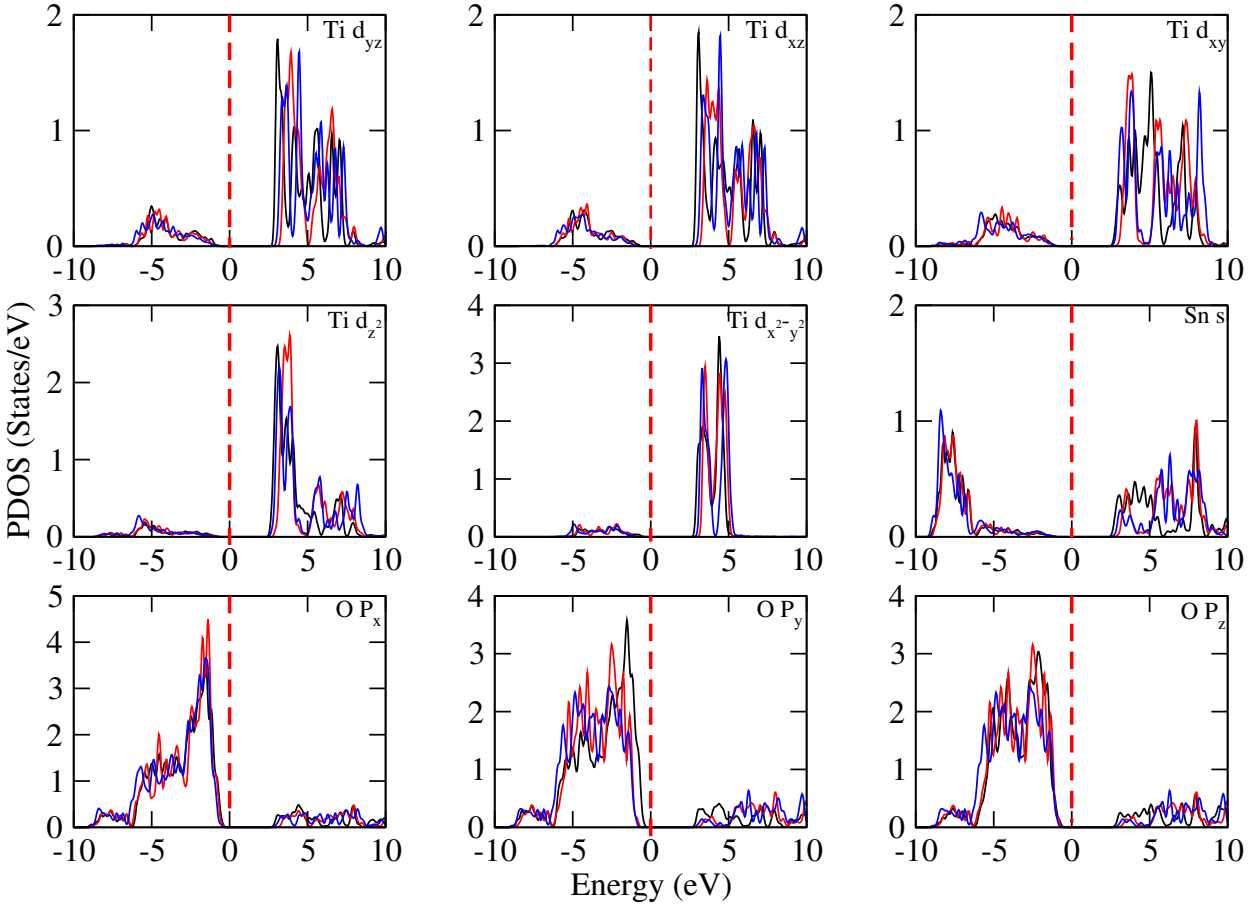

Figure S18: Ti-d, Sn-s and O-P orbital projected density of states of 1SO/1TO superlattices under upper limits -3% (black), 0% (red) and 4% (blue) biaxial strains.

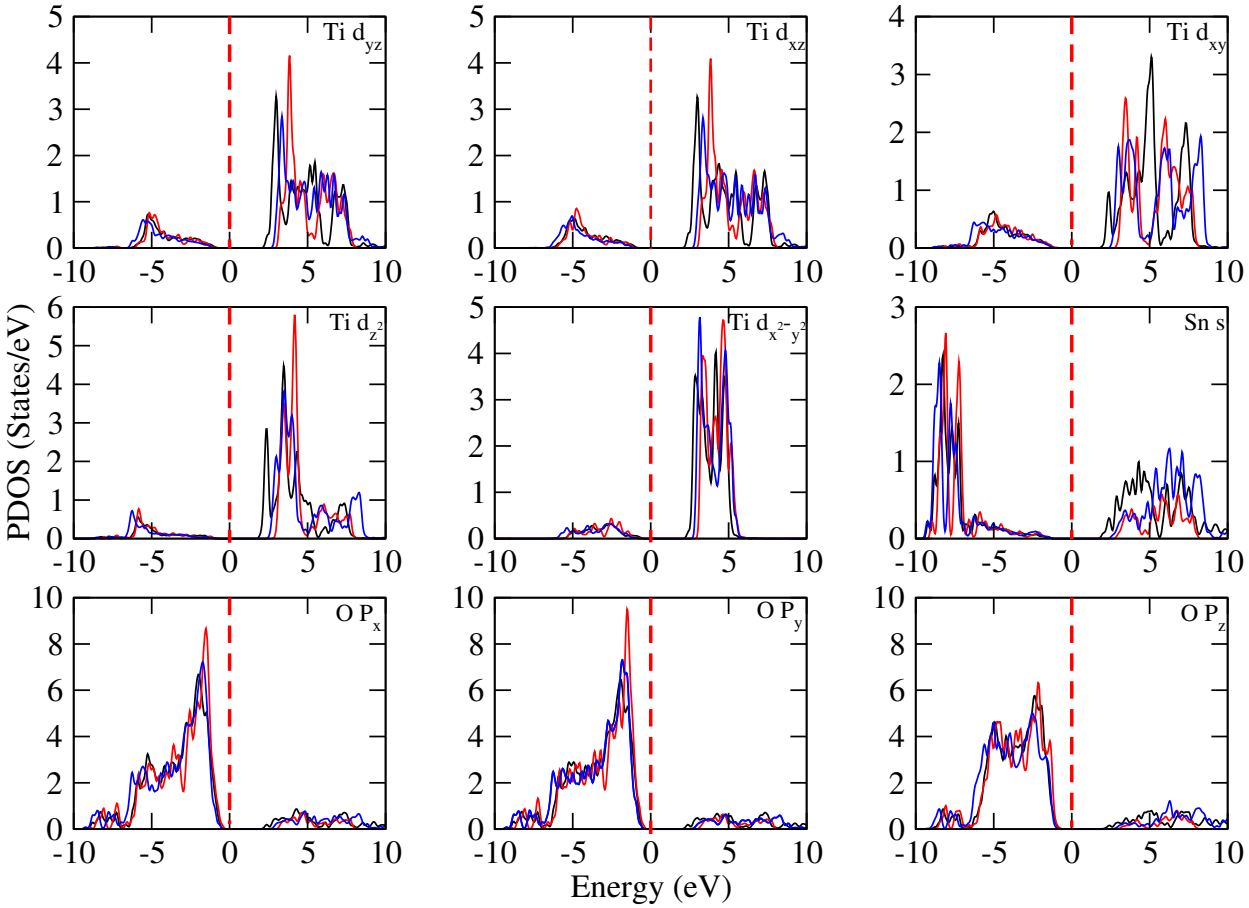

Figure S19: Ti-d, Sn-s and O-P orbital projected density of states of 2SO/2TO superlattices under upper limits 4% (black), 0% (red) and -3% (blue) biaxial strains.

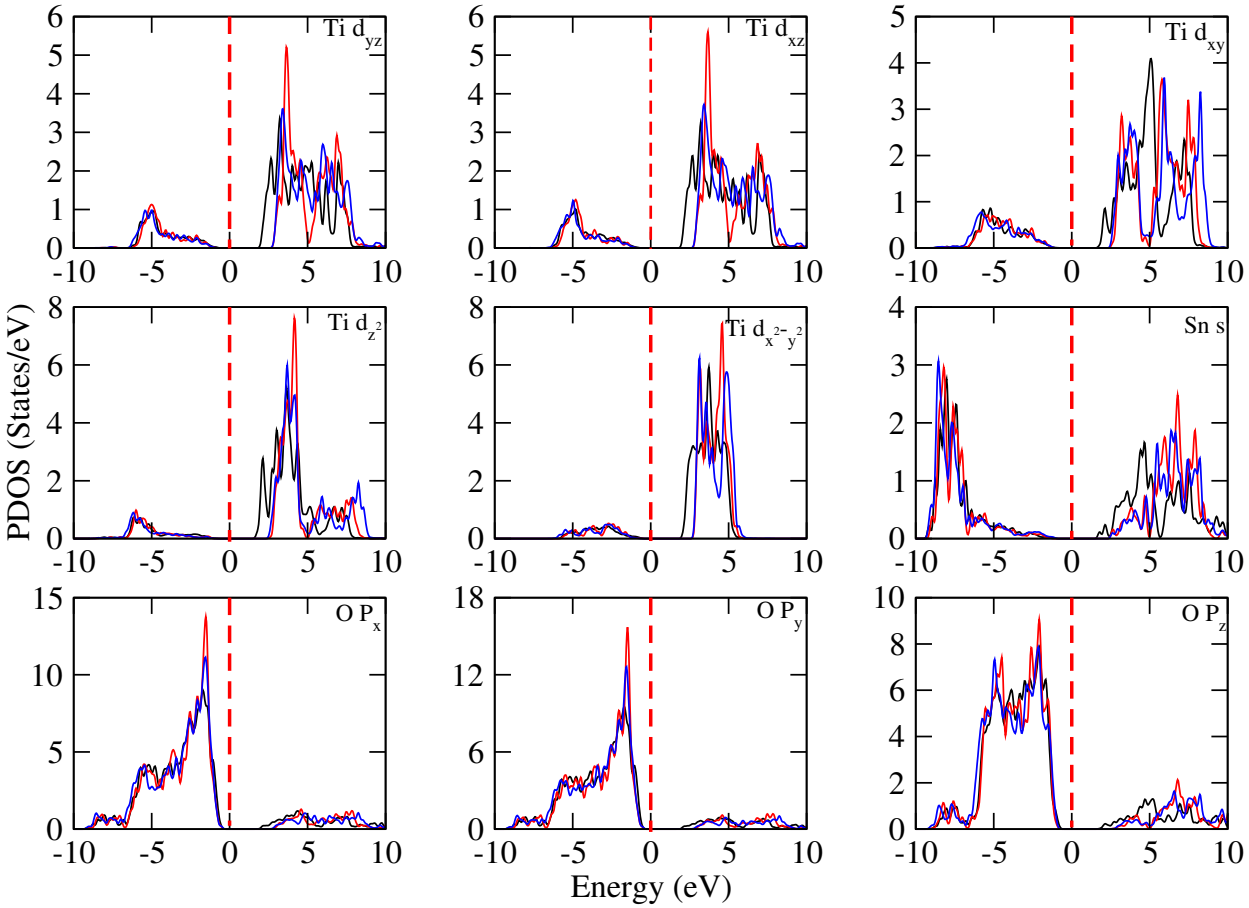

Figure S20: Ti-d, Sn-s and O-P orbital projected density of states of 3SO/3TO superlattices under upper limits 4% (black), 0% (red) and -3% (blue) biaxial strains

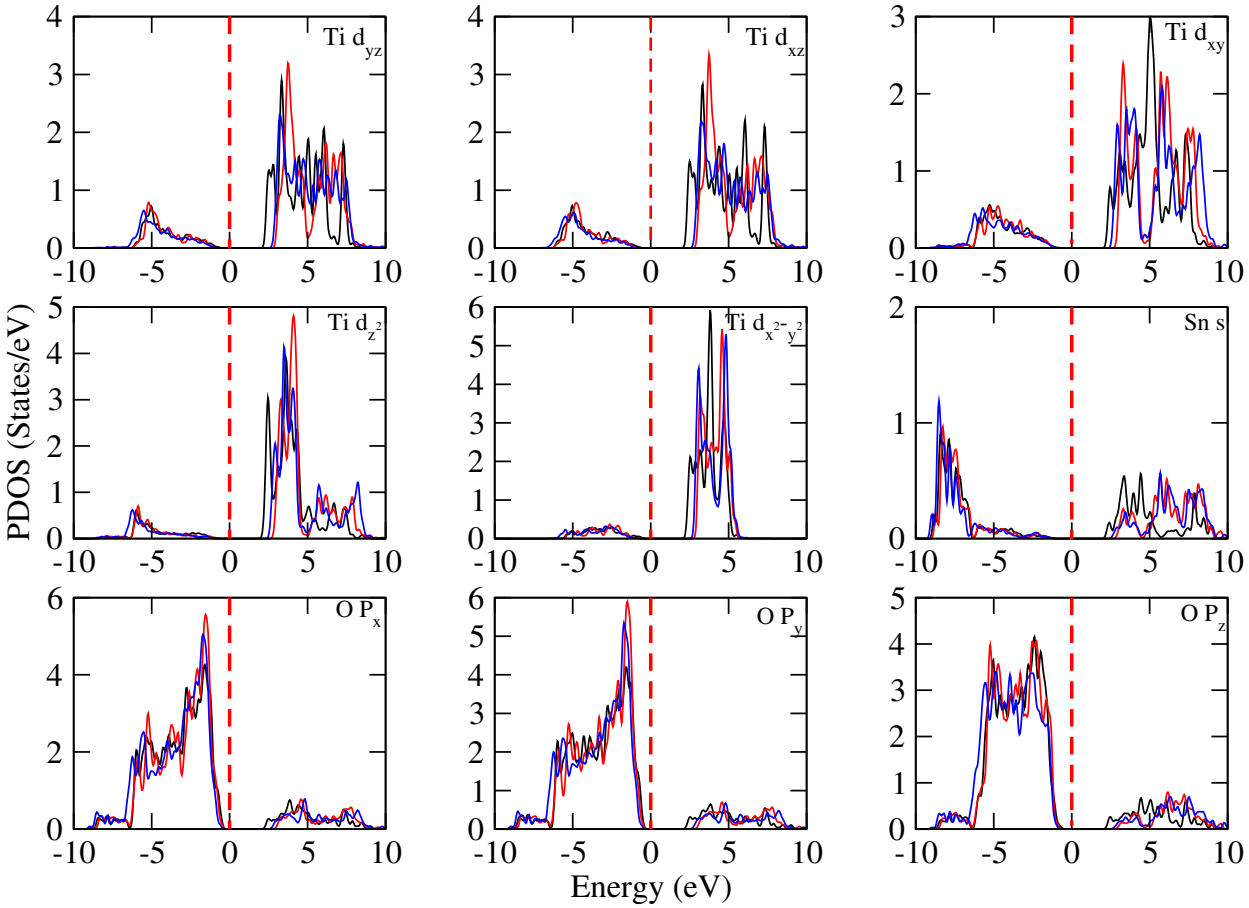

Figure S21: Ti-d, Sn-s and O-P orbital projected density of states of 1SO/2TO superlattices under upper limits -3% (black), 0% (red) and 4% (blue) biaxial strains.

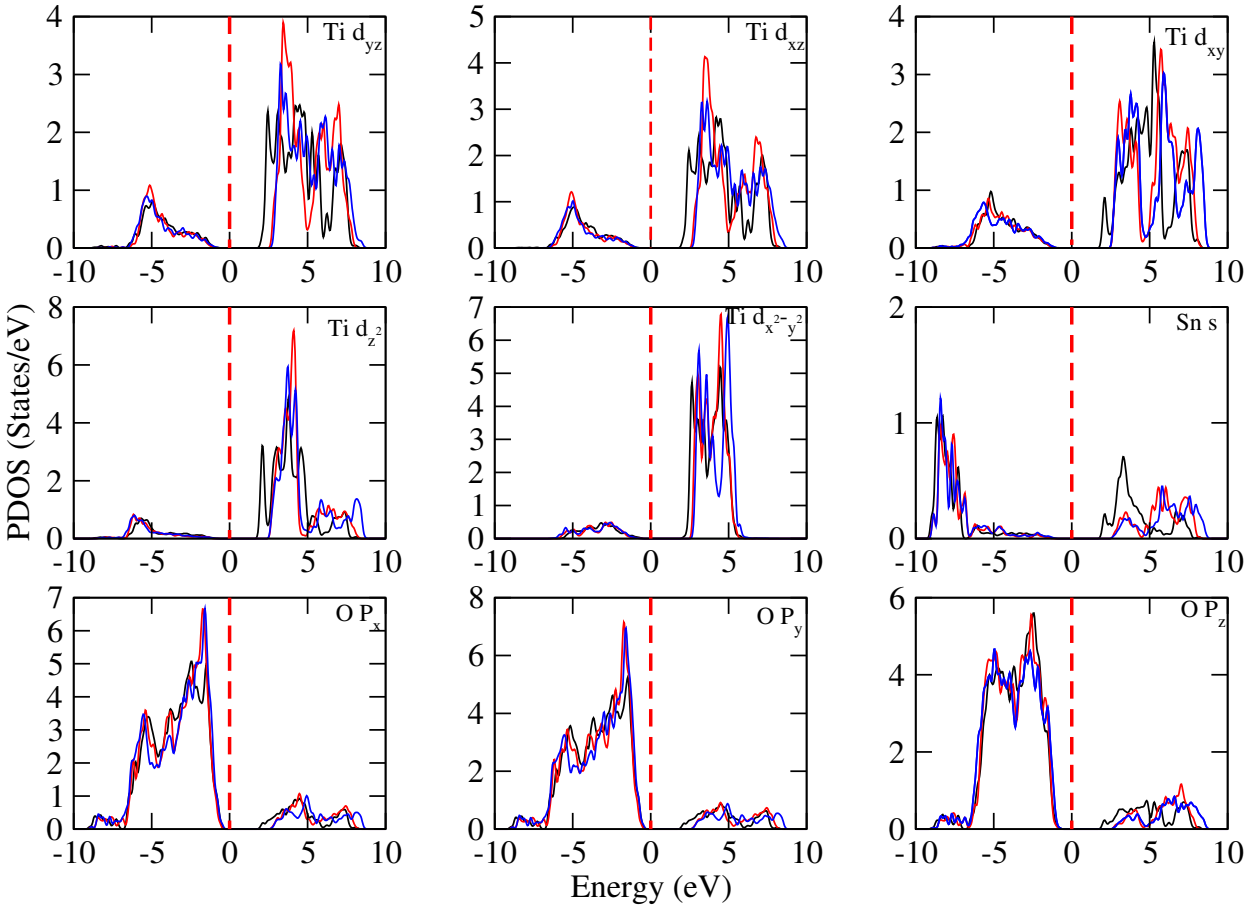

Figure S22: Ti-d, Sn-s and O-P orbital projected density of states of 1SO/3TO superlattices under upper limits -3% (black), 0% (red) and 4% (blue) biaxial strains.

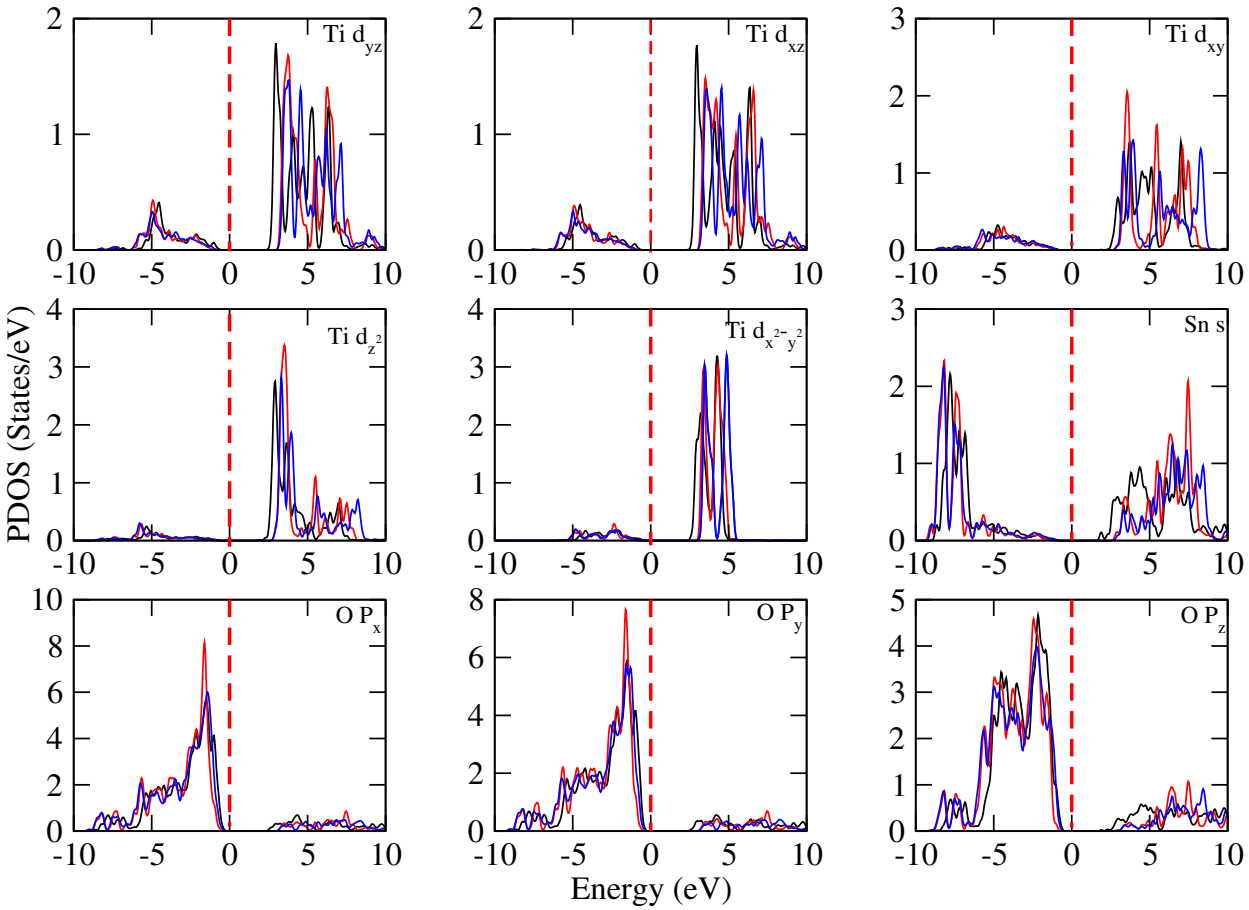

Figure S23: Ti-d, Sn-s and O-P orbital projected density of states of 2SO/1TO superlattices under upper limits -3% (black), 0% (red) and 4% (blue) biaxial strains.

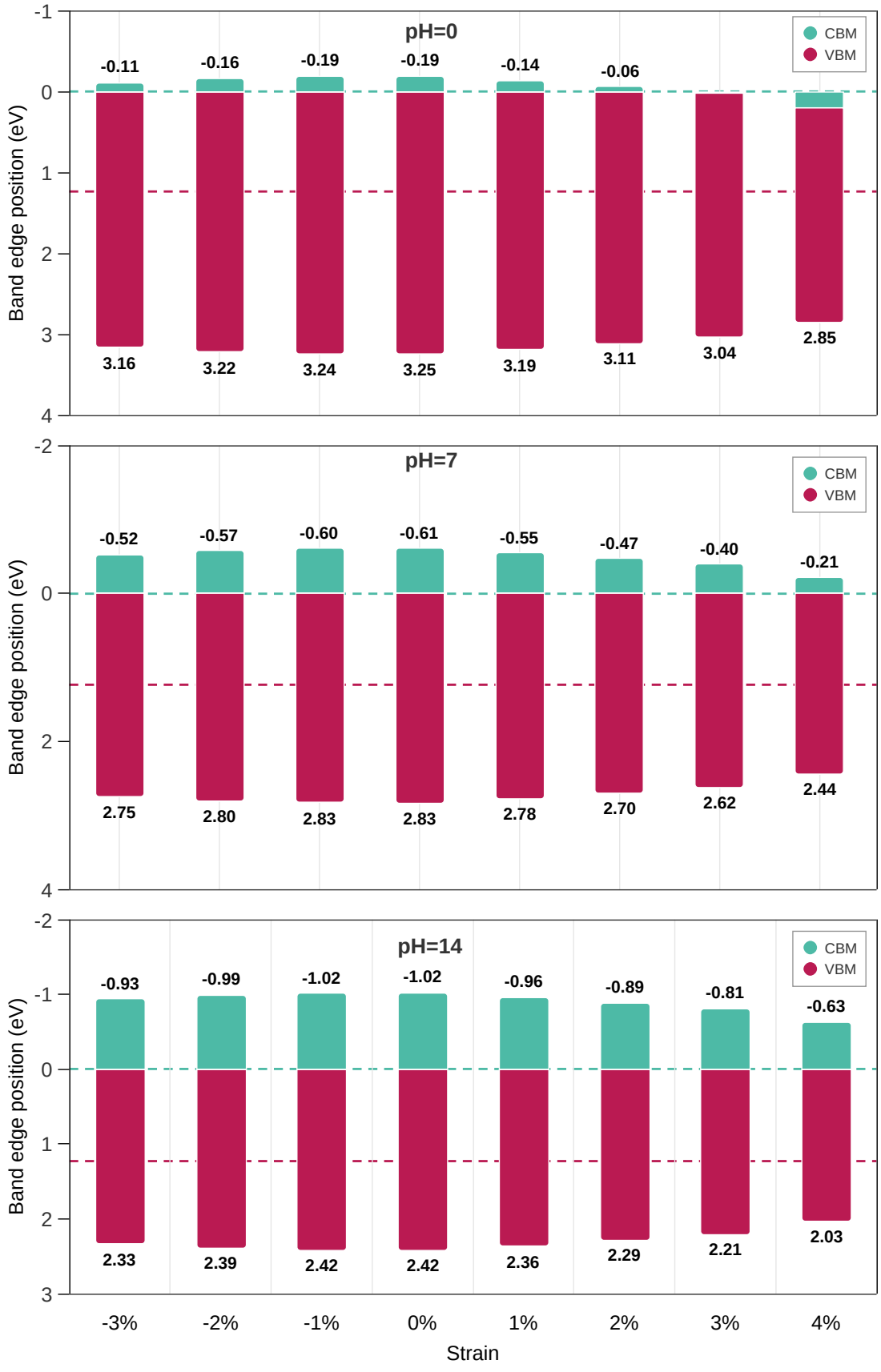

Figure S24: Energy alignment of $(SnO_2)_{(2)}/(TiO_2)_{(2)}$ superlattice under biaxial tensile and compressive strain when pH = 0 (upper part), 7 (middle part), and 14 (bottom part). The horizontal dashed lines are water redox potentials.

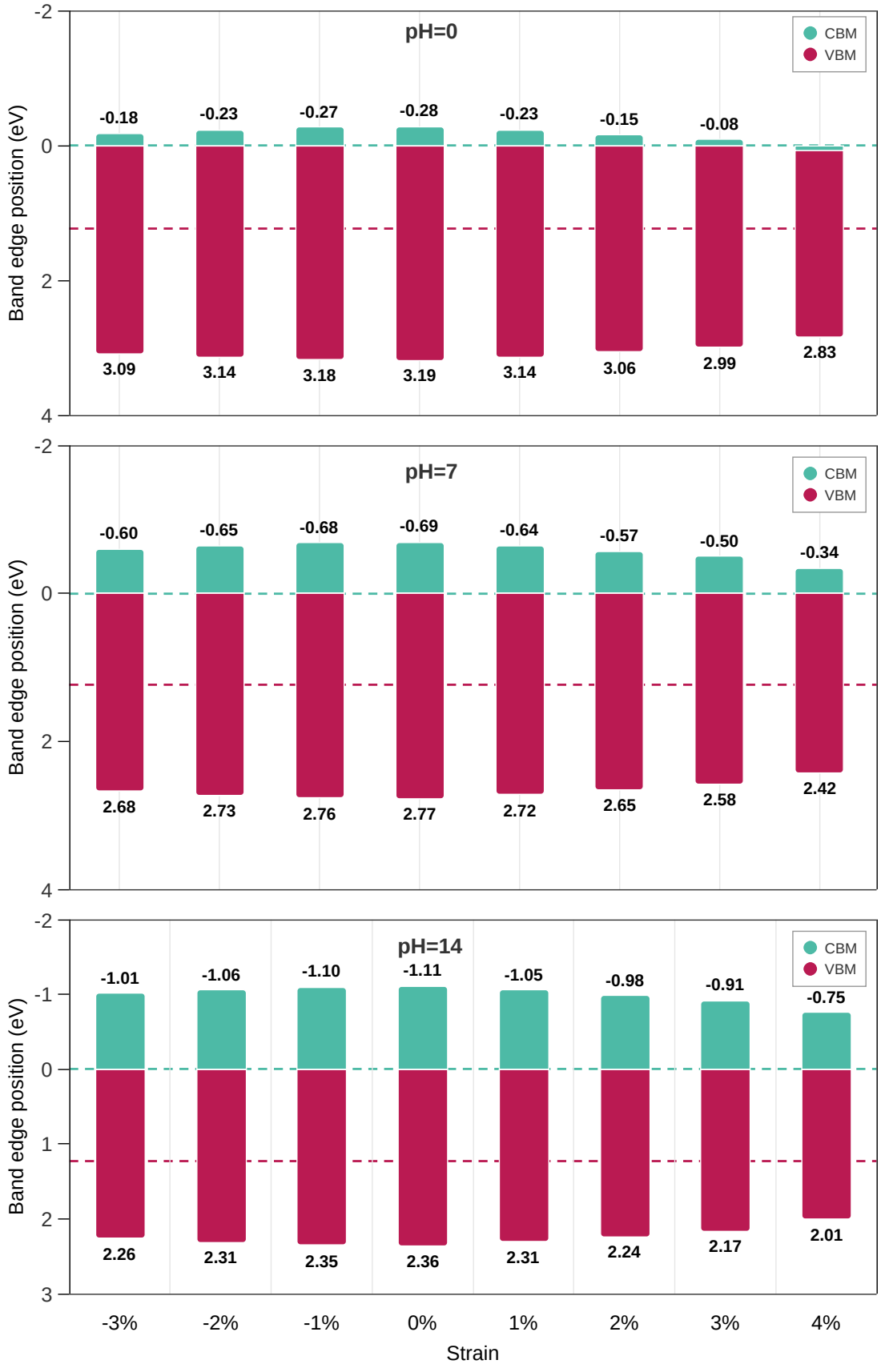

Figure S25: Energy alignment of $(SnO_2)_{(1)}/(TiO_2)_{(2)}$ superlattice under biaxial tensile and compressive strain when pH = 0 (upper part), 7 (middle part), and 14 (bottom part). The horizontal dashed lines are water redox potentials.

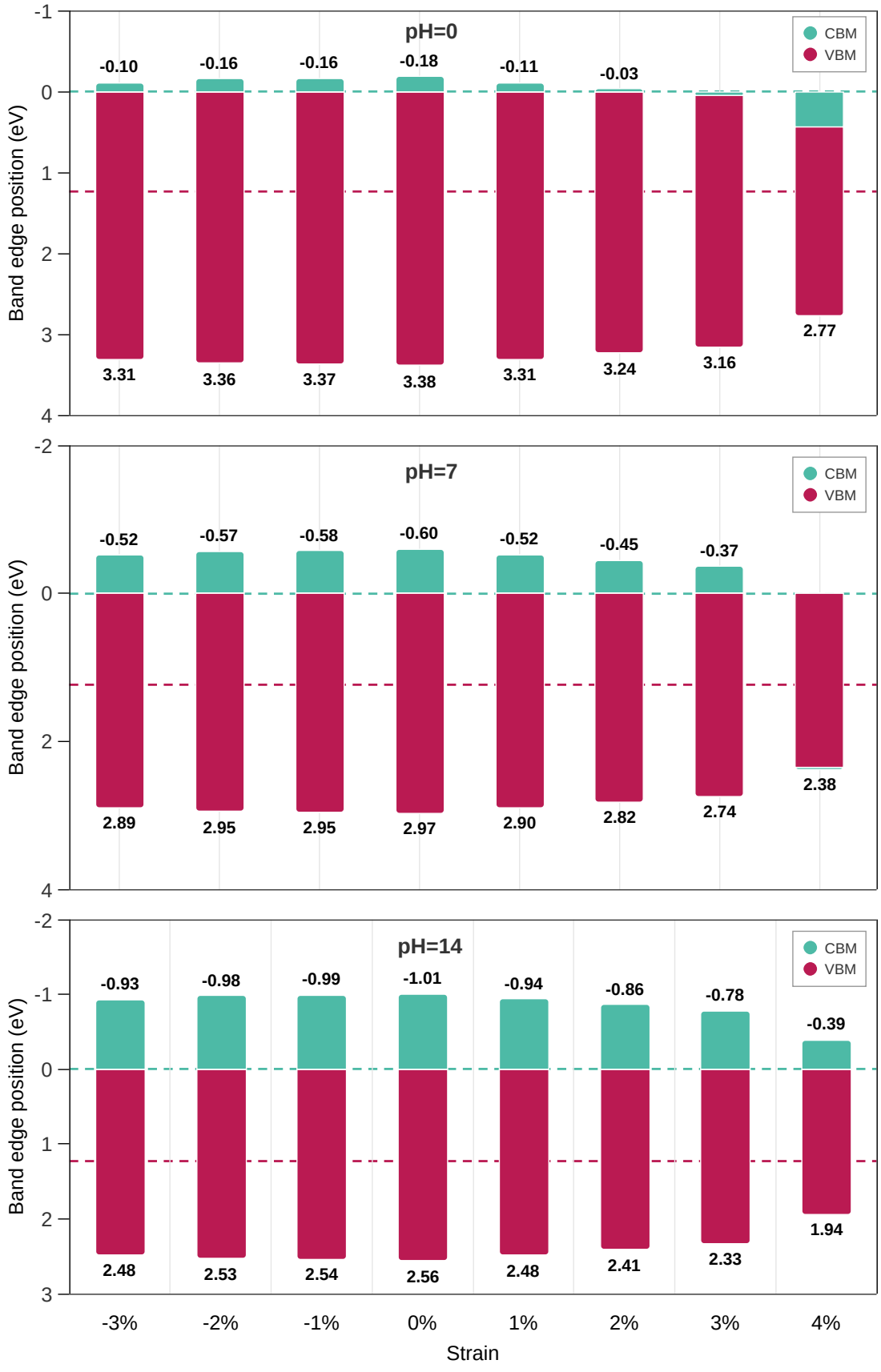

Figure S26: Energy alignment of $(SnO_2)_{(2)}/(TiO_2)_{(1)}$ superlattice under biaxial tensile and compressive strain when pH = 0 (upper part), 7 (middle part), and 14 (bottom part). The horizontal dashed lines are water redox potentials.

References

[1] Bo Thangaraju. Structural and electrical studies on highly conducting spray deposited fluorine and antimony doped sno2 thin films from sncl2 precursor. *Thin solid films*, 402(1-2):71–78, 2002.

[2] SC Abrahams and JL Bernstein. Rutile: normal probability plot analysis and accurate measurement of crystal structure. *The Journal of Chemical Physics*, 55(7):3206–3211, 1971.